Quantitative Theory of Nanowire and Nanotube Antenna Performance

Peter J. Burke, *Member, IEEE*, Shengdong Li, *Member, IEEE*, and Zhen Yu, *Member, IEEE*

***Abstract*—We present quantitative predictions of the performance of nanotubes and nanowires as antennas, including the radiation resistance, the input reactance and resistance, and antenna efficiency, as a function of frequency and nanotube length. Particular attention is paid to the quantum capacitance and kinetic inductance. We develop models for both far-field antenna patterns as well as near-field antenna-to-antenna coupling. In so doing, we also develop a circuit model for a transmission line made of two parallel nanotubes, which has applications for nanointerconnect technology. Finally, we derive an analog of Hallen's integral equation appropriate for single-walled carbon nanotube antennas.**

***Index Terms*—Antenna, nanotechnology, nanotube, nanowire.**

I. Introduction

WE RECENTLY demonstrated the operation of active nanotube devices at microwave (gigahertz) frequencies [1]. However, the electrical properties of nanotubes as passive high-frequency components such as interconnects [2], mixers, detectors [3], [4], and antennas are currently not well understood. In this paper, we study theoretically the interaction of one-dimensional electronic systems with microwave radiation, leading to a quantitative theory of nanowire and nanotube antenna performance. In our previous modeling work [5]–[8], we briefly considered nanotubes as antennas but did not quantitatively assess their performance potential. Recently, we have been able to synthesize and electrically contact single-walled carbon nanotubes (SWNTs) up to $\sim$1 cm in length [9], [10]. These tubes are comparable in length to the wavelength of microwaves in free space. This motivates our study of the interaction of microwaves with nanotubes and the exploration of their properties as antennas.

Nanotubes grown in our lab have conductivities several times larger than copper [9], [10], but the diameter is small, so the resistance is high. Thus, current nanotube growth technology allows for very lossy antennas. In spite of heavy losses, these may allow a wireless nonlithographic connection between nanoelectronic devices and the macroscopic world. If lower resistance nanotubes can be grown, we predict the antenna properties to be dramatically different from conventional thin-wire antennas.

Manuscript received August 8, 2004; revised April 6, 2006. This work was supported in part by the Office of Naval Research under Award N00014-02-1-0456, by the National Science Foundation under Contracts ECS-0300557 and CCF-0403582, by the Army Research Office under Award DAAD19-02-1-0387, and by the Defense Advanced Research Projects Agency under Award N66001-03-1-8914. The review of this paper was arranged by Associate Editor F. Terry.

The authors are with the Integrated Nanosystems Research Facility, Department of Electrical Engineering and Computer Science, University of California, Irvine, CA 92697-2625 USA (e-mail: pburke@uci.edu).

Digital Object Identifier 10.1109/TNANO.2006.877430

A. Limits of Applicability

The geometry we consider is that of a thin-wire center-fed antenna where the wire is made of a single-walled metallic carbon nanotube. This is the first step to a general theory of nanoantennas. Our calculations should also apply to semiconductor nanowire antennas in the quantum mechanical one-dimensional (1-D) limit and also to multiwalled nanotube (MWNT) antennas if suitably generalized [11]. MWNTs with scattering behavior interpreted as "optical antennas" were recently demonstrated [12]. Our theory applies only in the quantum mechanical 1-D limit, where only one subband is occupied by the electrons. Additionally, our theory assumes the excitation level is insufficient to promote electrons from one subband to another. If the excitation level is sufficiently high, then the system will no longer behave as a strictly 1-D system.

Therefore, this work does *not* apply to metallic "nanowires" (which are usually not in the 1-D quantum limit) or to semiconducting nanowires with more than one occupied subband. A possible future project would be to determine the crossover from nanoantenna to thin-wire antenna behavior. Some work in this intermediate regime has recently begun [13]–[15], and we discuss this crossover more extensively as follows.

Our work should apply in the microwave, submillimeter, and terahertz spectrum. In principle, our work can also apply in the IR and optical spectrum if the photon energy is lower than any electronic excitations at that energy.

B. Outline

This paper is divided up as follows. First, we discuss state-of-the art in nanotube synthesis, paying particular attention to nanotubes with length of the order of the wavelength of microwaves, i.e., centimeters [9], [10], [16]–[23]. Therefore, the synthesis of long SWNTs is possible in several laboratory settings.

Then, we discuss possible applications of nanotube antennas. Third, we present a circuit model for a two-nanotube transmission line, a necessary prestep for the following sections. Fourth, based on this circuit model, we calculate the spatial current distribution for a nanotube antenna. Once this current distribution is known, we treat each infinitesimal element of current as a radiator and add up (integrate) their contributions to the electric field to determine the total far-field electric field, hence radiated power. We do this first in the no ohmic loss case, then in the low ohmic loss case, and finally in the high ohmic loss case. We then go on to discuss the near-field coupling from one nanotube antenna to the next. Finally, we derive an integral equation (analogous to Hallen's integral equation) which outlines a general

technique for more precise numerical calculations of nanotube antenna performance.

Where possible, we provide executive summary-type conclusions of our calculations for performance predictions to researchers interested in building and measuring the performance of nanotube antennas. In what follows, we use the same terminology and symbol definition as our prior papers [5]–[8].

II. Nanotube Growth State-of-the-Art

In our lab, we have grown some of the longest electrically contacted SWNTs, with lengths up to 0.4 cm in length. Our measurements indicate that the resistance per unit length is around 6 $k\Omega/\mu$m. When scaled by the diameter of 1.5 nm, this gives rise to a three-dimensional (3-D) resistivity of 1 $\mu\Omega-$ cm, which is lower resistivity than copper. A similar conductivity was measured on 300-μm-long SWNTs by one other group [24]. Two other groups have been able to synthesize 600-μm [25] and several millimeters to 4.8-cm [16]–[22] SWNTs. Recent work has extended this to 10 cm [23]. Therefore, the synthesis of long SWNTs is possible in several laboratory settings.

For the resistance per unit length that we measured, as we will show, this would correspond to a very heavily damped antenna with significant ohmic losses. However, the mechanism for the scattering in long SWNTs is still not well studied. With sufficient effort, it may be possible to lower the resistance per length by improving the synthesis technique. Ultimately, if all impurities could be removed, phonon-scattering would prevail and limit any further lowering of the resistance and hence loss. At present, this ultimate limit is unknown. Therefore, the prospects for low-loss antennas are, at present, a long-term possibility.

III. Applications of Nanotube Antennas

A. Solution to Nanointerconnect Problem

Progress to date on nanoelectronics has been significant. Essentially, all devices needed to make the equivalent of a modern digital or analog circuit out of nanotubes and/or nanowires have been demonstrated in prototype experiments, and elementary logic circuits have been demonstrated [26]–[29].

However, one of the most important unsolved problems in nanotechnology is how to make electrical contact from nanoelectronic devices to the macroscopic world, without giving up on the potential circuit density achievable with nanoelectronics.

All of the nanotube and nanowire devices developed to date have been contacted by lithographically fabricated electrodes. A canonical research theme is to fabricate a nanodevice, contact it with electrodes fabricated with electron-beam lithography, then publish a paper reporting the electrical properties. This is not a scalable technique for massively parallel processing *integrated nanosystems*. The potential high-density circuitry possible with nanowires and nanotubes will not be realized if each nanowire and nanotube is contacted lithographically.

One potential solution to this problem is to use wireless interconnects, which can be densely packed. If each interconnect is connected to a nanotube of a different length (hence different resonant frequency), then the problem of multiplexing input/output signals can be translated from the spatial domain to the frequency domain, hence relaxing the need for high resolution (high cost) lithography for interconnects. This is in contrast to previous approaches which, ultimately, rely on lithography and its inherent limitations to make electrical contact to nanosystems. This idea is indicated schematically in Fig. 1.

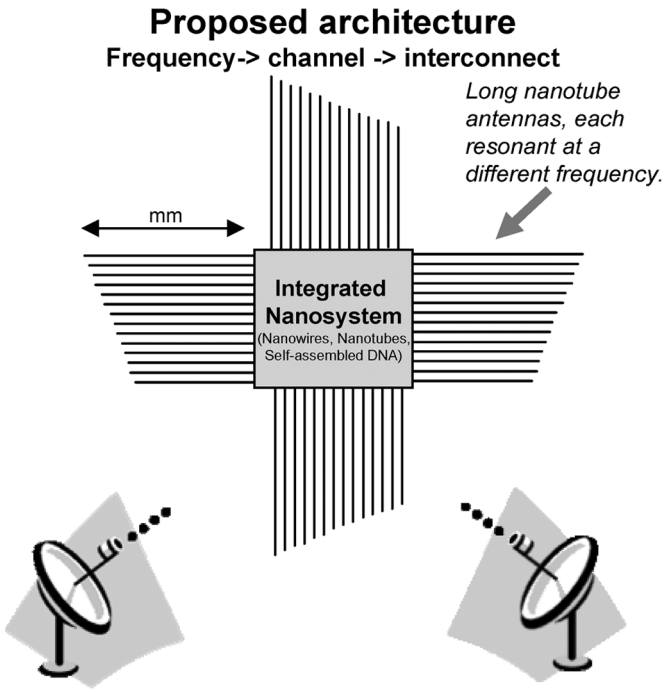

Fig. 1. Possible scheme for wireless interconnection to integrated nanosystems.

B. Wireless Interconnect to Nanosensors

Another application is in the area of sensing. For example, nanodevices could be use as chemical and biological sensors, sensitive to their local chemical environment. A nanotube could be used as an antenna to couple to these nanosensors, without the need for lithographically fabricated electronics. This would be an RFID technique, where each component of the wireless systems was made of a nanodevice, including the antenna, thus eliminating the need for any lithography at all. Such devices even potentially could be implanted into living organisms to monitor biological activity in real time *in vivo*.

IV. Two-Nanotube Transmission Line Properties

In order to understand the nanotube antenna performance, we must first develop an RF circuit model for a transmission line consisting of two parallel nanotubes. We first review the RF circuit model for an individual nanotube, then discuss the equivalent circuit model for two spinless 1-D wires, then discuss the circuit model appropriate for nanotubes, taking spin and band-structure degeneracy into account.

A. Single Nanotube RF Properties

In our recent papers [5]–[8], we considered the electrical properties of a SWNT above a ground plane in some detail. There, we found that, in addition to electrostatic capacitance and magnetic inductance, there were two additional distributed circuit elements to be considered: the quantum capacitance

and the kinetic inductance. We briefly reiterate their physical origins here.

The physical origin of the quantum capacitance comes from the finite density of states at the Fermi energy. In a quantum particle in a box, the spacing between allowed energy levels is finite. Because of this, to add an extra electron to the system takes a finite amount of energy above the Fermi energy. In 1-D systems, this can be equated with an energy per unit length. From this energy per unit length, a capacitance per unit length can be calculated. From [5]–[8], one finds the following expression for the (quantum) capacitance per unit length:

$$\mathcal{C}_Q = \frac{2e^2}{h v_F}. \tag{1}$$

The Fermi velocity for graphene and also carbon nanotubes is usually taken as $v_F = 8\,10^5$ m/s, so that numerically

$$\mathcal{C}_Q = 100\ \text{aF}/\mu\text{m}. \tag{2}$$

The kinetic inductance has a simple physical origin as well. It is due to the charge-carrier inertia: electrons due not instantaneously respond to an applied electric field; there is some delay. For periodic electric fields, the electron velocity lags the electric field in phase, i.e., the current lags the voltage in phase. This appears as an inductance. It can be shown [5]–[8] that in 1-D systems, this inductance is given by

$$\mathcal{L}_K = \frac{h}{2e^2 v_F} \tag{3}$$

which comes out to be numerically

$$\mathcal{L}_K = 16\ \text{nH}/\mu\text{m}. \tag{4}$$

This simple model has been put on more rigorous grounds in [30].

In a nanotube, there are four copropagating quantum channels: two spin-up channels and two spin-down channels. Each has its own kinetic inductance and quantum capacitance. All four channels have a common electrostatic capacitance to ground. This has a significant effect on the RF properties, as discussed in depth in [5]–[8].

B. Circuit Model for Two 1-D Wires of Spinless Electrons

In this section, we are interested in the differential modes of a two-nanotube transmission line system. There will be a voltage difference between the two nanotubes V(x,t) and a differential current I(x,t). For simplicity, consider two 1-D wires of diameter d separated by a distance W, as shown in Fig. 2. Each wire has its own kinetic inductance per unit length; we neglect the magnetic inductance because the kinetic inductance dominates.

There will be an electrostatic cross capacitance between the wires, which is defined as the voltage drop from one tube to the other when there is an excess charge on one tube and a decreased charge on the other tube. This can be calculated from simple electrostatics to be

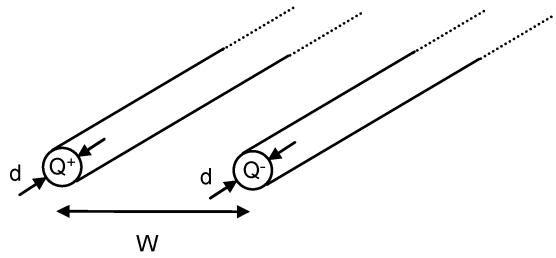

Fig. 2. Geometry of two-nanotube transmission line with differential mode excited.

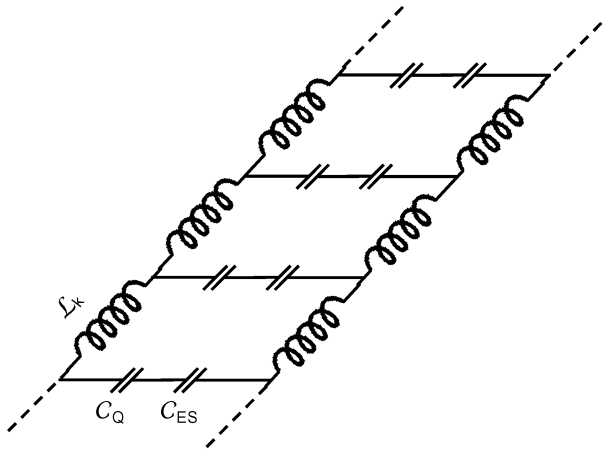

Fig. 3. RF circuit model for differential mode of two 1-D quantum wires with spinless electrons.

$$\mathcal{C}_{ES} = \frac{\pi\epsilon}{\cosh^{-1}(W/d)} \approx \frac{\pi\epsilon}{ln(W/d)}. \tag{5}$$

For the two-nanotube transmission line, the issue of the quantum capacitance deserves some attention. The correct way to include the quantum capacitance for the differential mode is shown in Fig. 3. This will be justified rigorously in a future manuscript. It is clear that the circuit model of Fig. 3 supports wave-like excitations of the current and voltage. Rather than calculating the wave properties explicitly, we move directly to the case of the two carbon nanotube transmissions line.

It should be noted that these discussions are meant to apply only to the differential mode. The common mode exication (where each nanotube carries the same charge) is not discussed here.

C. Circuit Model for Two Carbon Nanotubes

The circuit model for carbon nanotubes is more complicated, since each nanotube has four channels (two spin up, two spin down), each with its own kinetic inductance and quantum capacitance. For the differential mode excitations considered herein, the effective circuit model is modified. There are two spin orientations and two band structure channels that can propagate current, i.e., four 1-D quantum channels in parallel. Therefore, the kinetic inductance is four times lower than the one-channel

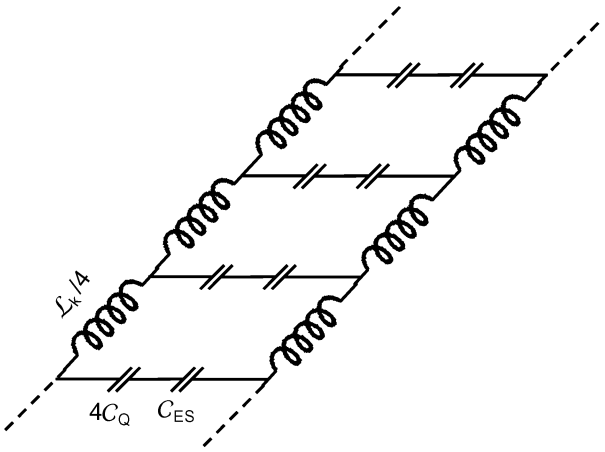

Fig. 4. RF circuit model for differential mode of two-nanotube transmission line.

case, and the quantum capacitance is four times higher than the one-channel case. The effective circuit diagram that takes these into account is given in Fig. 4.

By simple applications of Kirchoff's laws to the circuit shown in Fig. 4, we can come up with a differential equation for the differential voltage. If we write the voltage and current on tube 1 as V_1 and I_1, and the voltage and current on tube 2 as V_2 and I_2, and define the differential voltages and currents (assuming a harmonic time dependence) as

$$V_D \equiv V_1 - V_2 \tag{6}$$
$$I_D \equiv I_1 - I_2 \tag{7}$$

then the following differential equation holds:

$$\frac{\partial^2 V_D}{\partial x^2} - \gamma_p^2 V_D = 0 \tag{8}$$

where the propagation constant is given by

$$\gamma_p^2 \equiv 2(\mathcal{R} + i\omega\mathcal{L}_K/4)(i\omega\mathcal{C}_{\text{Total}}). \tag{9}$$

Here, we have introduced $\mathcal{R}$ as the resistance per unit length for a single tube in order to account for possible damping; this will be discussed in depth. We use the subscript "p" for plasmon, because these excitations are collective oscillations of the 1-D electron density, i.e., plasmons.

General solutions for the differential current and voltage can be written as

$$V_D(x) = V_0^+ e^{-\gamma_p x} + V_0^- e^{\gamma_p x} \tag{10}$$
$$I_D(x) = I_0^+ e^{-\gamma_p x} + I_0^- e^{\gamma_p x} \tag{11}$$
$$= \frac{V_0^+}{Z_C} e^{-\gamma_p x} - \frac{V_0^-}{Z_C} e^{\gamma_p x} \tag{12}$$

where the characteristic impedance and wave velocity are given by

$$Z_C \equiv \frac{1}{\sqrt{2}} \sqrt{\frac{\mathcal{R} + i\omega\mathcal{L}_K/4}{i\omega\mathcal{C}_{\text{Total}}}} \tag{13}$$
$$v_p \equiv \frac{1}{\sqrt{2}} \frac{1}{\sqrt{(\mathcal{L}_K/4)\mathcal{C}_{\text{Total}}}} \tag{14}$$

with

$$\mathcal{C}_{\text{Total}}^{-1} = (4\mathcal{C}_Q)^{-1} + \mathcal{C}_{ES}^{-1}. \tag{15}$$

The characteristic impedance is so defined because the ratio of the voltage to the current is constant for a given propagation direction, i.e.,

$$\frac{V_0^+}{I_0^+} = -\frac{V_0^-}{I_0^-} = Z_C. \tag{16}$$

Numerically, for typical cases, we have

$$Z_C \approx \frac{h}{2e^2} = 12\,\text{k}\Omega \tag{17}$$
$$v \approx v_{\text{Fermi}} \approx 0.01\,\text{c}. \tag{18}$$

Note that we are only considering the differential mode here. There will also be common mode excitations, which will be wave-like as well. We do not discuss those here, nor do we claim that our circuit model is appropriate for common mode excitations.

D. Discussion

First, we neglected the magnetic inductance, which is justified because it is numerically much smaller than the kinetic inductance.

Second, the wave velocity of this system is about 100 times smaller than the speed of light. This is because of the excess kinetic inductance.

Third, the existence of wave-like current excitations is well documented in the theoretical physics literature on 1-D quantum systems [31]–[39]. Such slow-wave structures have been confirmed at gigahertz frequencies using two dimensional (2-D) systems with kinetic inductance much larger than magnetic inductance by experiments performed by some of us [40]–[42].

Fourth, our paper is the first to consider the coupled nanotube transmission line. This should be put on more rigorous theoretical grounds by theoretical physicists, who would find an in-phase and out-of-phase coupled charge oscillation mode. Similar work has been done already on closely spaced 2-D electron gas systems [43]. Our circuit model describes the out of phase (differential) mode.

Fifth, the propagation constant and characteristic impedance are general expressions that take into account loss. In the low-loss case, they reduce to the more familiar forms. However, the

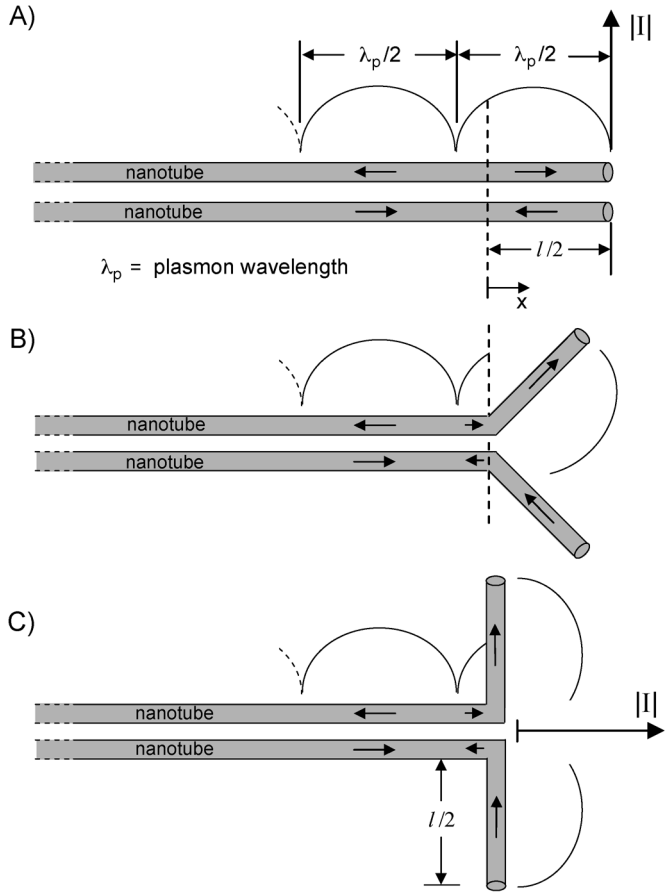

Fig. 5. Flaring. λ_p is plasmon wavelength, which is different than free-space wavelength λ.

previous expressions are completely general, including the case of high and low loss.

V. Current Distribution on Nanotube Antenna

A. Qualitative Discussion

Fig. 5 shows the standard textbook geometry to calculate the current distribution on a classical thin-wire antenna [44]. However, in our case, due to the kinetic inductance and quantum capacitance, the wave velocity is very different from a classical thin-wire antenna, where only the magnetic inductance is present.

In Fig. 5(a), we consider the excited two-nanotube transmission line, where the ends are open. In this case, a standing-wave pattern is built up (as indicated) for the current and voltage along the two-nanotube transmission line. Because the currents on the two nanotubes are in equal and opposite direction, the far-field magnetic and electric fields generated by each of the wires individually cancels. Therefore, the radiated power is approximately zero.

In Fig. 5(b), we consider "flaring" the two ends. If the flaring angle is small, the transmission line properties are almost the same, hence the standing wave pattern in the current is unchanged. However, because the wires are no longer close to each other at the ends, the far-field electric and magnetic fields generated by the wires near the end do not cancel, hence the system radiates power. Eventually, the flare angle becomes 90°, and that is the geometry considered in this paper. The currents are quantitatively calculated as follows.

Note that the technology to fabricate such flared geometries is not currently available. In addition, the symmetry of the flare will have an important (critical) effect on the input impedance of the antenna.

B. Second-Order Flaring Effects

The wave velocity for a traditional two-parallel wire transmission line is independent of the distance between the wires and equal to the speed of light. Because of this, it is usually assumed that the current distribution for the flared two-nanotube system has the same wavelength as the unperturbed two-wire transmission line.

For two-wire nanotube transmission lines, the wave-velocity depends on the distance between the nanotubes. Therefore, the wave velocity for the flared nanotubes is different. The reason is simple: the kinetic inductance does not depend on the distance between the tubes; whereas, the capacitance does. Therefore, the wave velocity $\sim 1/\sqrt{LC}$ depends on the distance between the tubes. This means that for the 90° flared nanotubes, the wavelength of the current distribution is different. However, since the electrostatic capacitance is only sensitive to the log of the distance between nanotubes, this effect will be neglected herein. Therefore, we will assume that the current distribution of the flared nanotubes [Fig. 5(c)] is the same as that of the unflared nanotubes [Fig. 5(a)]. We now calculate that current distribution.

C. Quantitative Prediction for Arbitrary Resistance

We can use the transmission-line equations to develop expressions for the current distribution on the wire, explicitly and quantitatively including the effect of resistance along the tube, but neglecting (for the moment) the radiation resistance. If there is a positive-going voltage wave of amplitude V_0^+, it will be reflected off of the ends of the transmission line, with reflection coefficient 1 (since the ends are an open circuit). Therefore, there will be a negative-going voltage wave of amplitude V_0^- of equal amplitude. The propagation constant is γ_p.

The voltage along the antenna can be expressed then as

$$V_D(x) = V_0^+ e^{-\gamma_p(x-l/2)} + V_0^- e^{\gamma_p(x-l/2)} \tag{19}$$

$$= V_0^+ e^{-\gamma_p(x-l/2)} + V_0^+ e^{\gamma_p(x-l/2)} \tag{20}$$

$$= 2V_0^+ \cosh\left[\gamma_p(x-l/2)\right]. \tag{21}$$

Note that, in this notation, the voltage at the terminals of the antenna $V_{\text{terminals}}$ is related to the amplitude of the positive going voltage wave V_0^+ by

$$V_{\text{terminals}} = 2V_0^+ \cosh\left[\gamma_p(l/2)\right]. \tag{22}$$

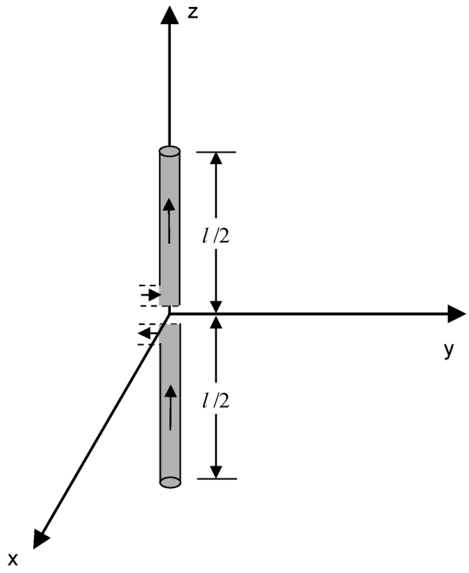

Fig. 6. Antenna geometry.

We can use (12) to find the differential current on the line, and it is given by

$$I_D(x) = \frac{V_0^+}{Z_C} e^{-\gamma_p (x - l/2)} - \frac{V_0^-}{Z_C} e^{\gamma_p (x - l/2)} \tag{23}$$

$$= \frac{V_0^+}{Z_C} e^{-\gamma_p (x - l/2)} - \frac{V_0^+}{Z_C} e^{\gamma_p (x - l/2)} \tag{24}$$

$$= \frac{2V_0^+}{Z_C} \sinh\left[\gamma_p (l/2 - x)\right]. \tag{25}$$

This is referred to in Fig. 5, before flaring. After flaring, the detailed geometry is shown in Fig. 6. It is clear from inspection that both I_1 and I_2 are in the same direction (the positive z direction), and each will be equal to half of I_D. Therefore, the current on the active region of the antenna can be written as

$$\mathrm{I}(z) = \begin{cases} \frac{V_0^+}{Z_C} \sinh\left[\gamma_p (l/2 - z)\right] & 0 < z < l/2 \\ \frac{V_0^+}{Z_C} \sinh\left[\gamma_p (z + l/2)\right] & 0 > z > -l/2. \end{cases} \tag{26}$$

These equations describe the nanotube antenna current distribution for arbitrary loss, neglecting the radiation resistance.

In the absence of loss (i.e., $\mathcal{R} = 0$), the current can be written as

$$\mathrm{I}(z) = \begin{cases} I_0 \sin\left[k_p (l/2 - z)\right] & 0 < z < l/2 \\ I_0 \sin\left[k_p (z + l/2)\right] & 0 > z > -l/2 \end{cases} \tag{27}$$

where k_p is real and equal to ω/v_p, the plasmon velocity given by (14), and $I_0 \equiv iV_0^+/Z_C$. This is what distinguishes a nanotube antenna from a traditional antenna, where the wavevector for the current is the same as the free-space wave vector.

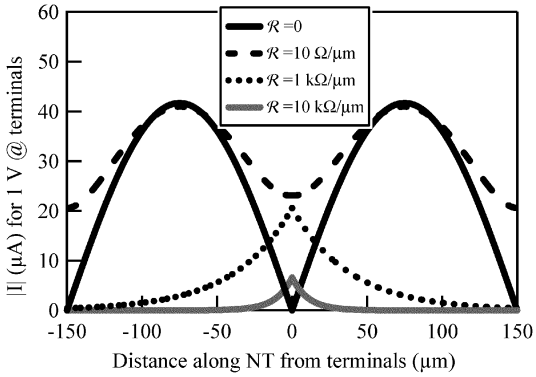

Fig. 7. Current distribution for 1-V 10-GHz excitation on 300-μm antenna.

In Fig. 7, we plot the magnitude of the ac current as a function of position for various values of R, for a 10-GHz frequency and 300-μm-long nanotube antenna, for a voltage at the terminals of $V_{\text{terminals}} = 1$ V. For low enough $\mathcal{R}$, the current distribution is approximately sinusoidal. As $\mathcal{R}$ increases, the resonance behavior gives rise to an amplitude that decays exponentially with distance from the terminals.

D. Effect of Radiation on Current Distribution

We will calculate the far-field electric fields generated by the current distribution given in (26) and (27). This is not entirely self-consistent, because the current distribution expression given by (26) and (27) neglect radiation. In reality, there will be a change in the current distribution due to the radiation. The far-field electric fields and the current distribution are related through a set of integro-differential equations, which can only be solved numerically. However, generally speaking, for thin wire antennas the current distribution is only slightly modified by the radiation and is usually neglected. In this paper, we will assume the current distribution is not significantly changed by the radiation. This assumption should be put on more rigorous grounds in future work, but seems reasonable given what is known about traditional thin wire antennas.

In summary, we will neglect the effect of radiation on the current distribution and take (26) and (27) as a given for the rest of this paper; we turn to the consequences of this current distribution on radiation, hence antenna properties.

VI. Radiation Properties Under No-Loss Conditions

Once the current distribution is known, we can treat each infinitesimal element of current as a radiator and add up (integrate) the contributions to determine the far-field electric field. In this section, we will discuss the no-loss condition. While this may not be achievable in practice, it gives information about the "ideal" case.

A. Electric Field

Based on the known current distribution, it is straightforward to calculate the radiated electric and magnetic fields. We follow Balanis [44]. For a wire antenna of arbitrary current distribution

I_e along the z axis, the electric field in the far field region is in the θ direction and given by

$$E_\theta = i\eta \frac{ke^{-ikr}}{4\pi r} \sin\theta \left[\int_{-l/2}^{+l/2} I(z) e^{ikz\cos\theta} dz \right]. \quad (28)$$

Here, η is the characteristic impedance of free space, equal to $120\pi\ \Omega$.

The key result of this paper is that while for a traditional wire antenna the current distribution is periodic with wave-vector given by $k = 2\pi/\lambda$, where λ is the free-space electromagnetic wavelength, for a nanotube the current is periodic with wavevector given by $k = 2\pi/\lambda_p$, where λ_p is the plasmon wavelength. This causes the integral of (28) to be different from a traditional thin-wire antenna.

Numerically, $k_p \approx 100k$, i.e., $\lambda_p \approx 1/100\lambda$, where λ is the free-space wavelength. For simplicity, we will assume this relationship to be exact from now on.

We can write the electric field as

$$E_\theta = i\eta \frac{ke^{-ikr}}{4\pi r} \sin\theta X \left\{ \int_{-l/2}^{0} I_0 \sin\left[k_p\left(\frac{l}{2}+z\right)\right] e^{ikz\cos\theta} dz + \int_{0}^{+l/2} I_0 \sin\left[k_p\left(\frac{l}{2}-z\right)\right] e^{ikz\cos\theta} dz \right\}. \quad (29)$$

Equation (29) can be evaluated, and the result is

$$E_\theta = i\eta \frac{k}{k_p} \frac{I_0 e^{-ikr}}{2\pi r} \sin\theta \frac{\cos\left(\frac{kl}{2}\cos\theta\right) - \cos\left(\frac{k_p l}{2}\right)}{1-(k/k_p)^2\cos^2\theta}. \quad (30)$$

B. Poynting Vector and Radiation Intensity

The Poynting vector can be calculated from the electric field, resulting in

$$\vec{W}_{\rm av} = \hat{r}\frac{1}{2\eta}|E_\theta|^2 \quad (31)$$

$$= \left(\frac{k}{k_p}\right)^2 \frac{I_0^2\eta}{8\pi^2 r^2} \times \left[\sin\theta \frac{\cos\left(\frac{kl}{2}\cos\theta\right) - \cos\left(\frac{k_p l}{2}\right)}{1-(k/k_p)^2\cos^2\theta}\right]^2. \quad (32)$$

Next, the (time-average) radiation intensity can be written as

$$U = r^2 W_{\rm av} \quad (33)$$

$$= \left(\frac{k}{k_p}\right)^2 \frac{I_0^2\eta}{8\pi^2} \left[\sin\theta \frac{\cos\left(\frac{kl}{2}\cos\theta\right) - \cos\left(\frac{k_p l}{2}\right)}{1-(k/k_p)^2\cos^2\theta}\right]^2. \quad (34)$$

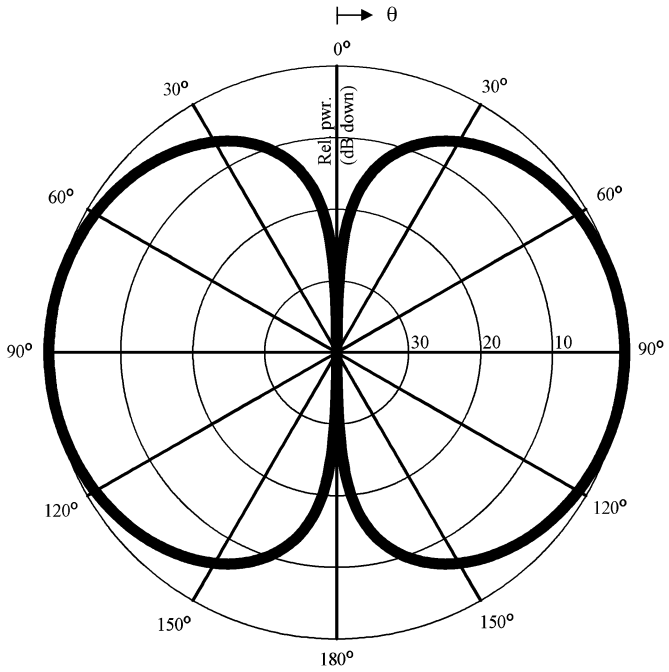

Fig. 8. E-plane antenna pattern, based on (30). We assume $k_p l/2 = \pi$.

The antenna pattern is similar to a regular wire antenna as long as the length is not near $l/\lambda = 0.02\,n$, with n an integer. (We remind the reader the λ is the electromagnetic radiation wavelength, which is about 100 times smaller than λ_p, the wavelength of the current excitation.) If the length is near one of these multiples, the pattern develops extra lobes. (This includes the case that the electrical length exceeds the full-wavelength λ_p.) In any case, (34) contains the full radiation pattern for arbirtrary frequencies and antenna lengths. The radiation pattern is plotted in Fig. 8 for the particular case of $l/\lambda = 0.01$, i.e., $l/\lambda_p = 1$.

C. Total Radiated Power

The total radiated power can be determined by integrating the radiation intensity over a sphere, i.e.,

$$P_{\rm rad} = \oint_S \vec{W}_{\rm av} \cdot d\vec{s}$$

$$= \int_0^{2\pi}\int_0^{\pi} W_{\rm av} r^2 \sin\theta d\theta d\phi$$

$$= \left(\frac{k}{k_p}\right)^2 \frac{I_0^2\eta}{4\pi} \times \int_0^{\pi} \sin^3\theta \left[\frac{\cos\left(\frac{kl}{2}\cos\theta\right) - \cos\left(\frac{k_p l}{2}\right)}{1-(k/k_p)^2\cos^2\theta}\right]^2 d\theta \quad (35)$$

$$= \left(\frac{k}{k_p}\right)^2 \frac{I_0^2\eta}{2} \xi(kl, k_p l) \quad (36)$$

where we have defined the function $\xi(kl, k_p l)$ as

$$\xi(kl, k_p l) \equiv \frac{1}{2\pi} \int_0^{\pi} \sin^3\theta \left[\frac{\cos\left(\frac{kl}{2}\cos\theta\right) - \cos\left(\frac{k_p l}{2}\right)}{1 - (k/k_p)^2 \cos^2\theta} \right]^2 d\theta. \tag{37}$$

The function $\xi(kl, k_p l)$ can be evaluated numerically. The function ξ is of the order of unity and plotted in Appendix I. It is periodic with $k_p l$.

D. Radiation Resistance

The radiation resistance is defined by

$$R_r \equiv \frac{2P_{\text{rad}}}{|I_0|^2} = \left(\frac{k}{k_p}\right)^2 \eta \xi(kl, k_p l). \tag{38}$$

Since ξ is of the order of unity, the radiation resistance is of the order $\eta/10^4 = 0.04\,\Omega$.

E. Directivity and Effective Aperture

The directivity is given by the maximum value of the radiated intensity divided by its average value, i.e.,

$$D = \frac{W_{\text{av}}|_{max}/A}{\oint_S \vec{W}_{\text{av}} \cdot d\vec{s}}. \tag{39}$$

We have numerically evaluated D as a function of kl and find that it is two, as long as the length is not near $l/\lambda = 0.02\,n$, with n an integer. The pattern is that of a simple thin-wire dipole radiator. If the length is near one of these multiples, the pattern develops extra lobes, and in that case the directivity can be as high as 5–6. In Appendix II, we plot the directivity determined numerically as a function of kl.

The effective area is related to the directivity through

$$A_{\text{eff}} = \frac{\lambda^2}{4\pi} D. \tag{40}$$

Therefore, for most values of kl, the effective area is approximately given by

$$A_{\text{eff}} \approx \frac{\lambda^2}{2\pi}. \tag{41}$$

This is similar to a thin-wire antenna.

F. Input Impedance

The radiation resistance relates the power radiated to I_0, the maximum amplitude of the current along the nanotube. However, the current at the terminals is equal to $I_0 \sin(k_p l/2)$. The input resistance due to radiation R_{in} is related to the power dissipated due to radiation through $P_{\text{rad}} = I^2 R_{\text{in}}$, where R_{in} is the current at the terminals. Therefore, taking this into account, the input resistance (when there is no intrinsic loss) is given by

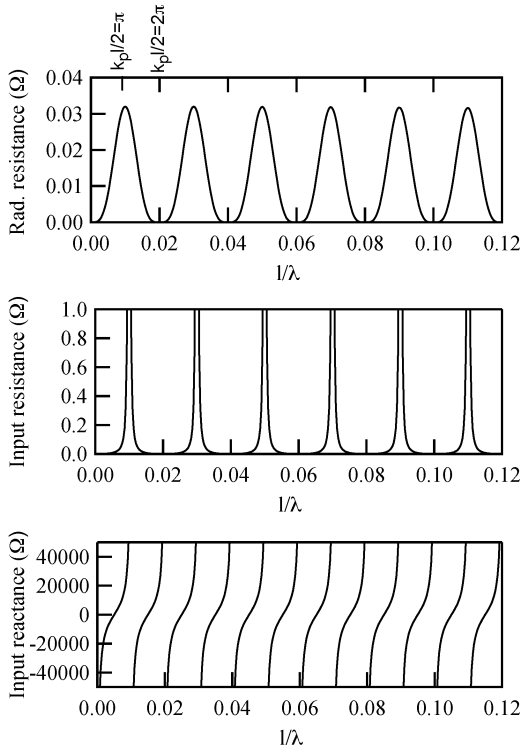

Fig. 9. Plot of radiation resistance, input resistance, and input reactance as function of l/λ, where λ is free-space wavelength, assuming that $k_p = 100k$. x axis is $l/\lambda = kl/2\pi = 0.01 k_p l/2\pi$.

$$R_{\text{in}} = \frac{R_r}{\sin^2(k_p l/2)}. \tag{42}$$

The input reactance is easy to understand from Fig. 5 as the input impedance of a two-nanotube transmission line of length l/2. This is given by

$$Z_{\text{in}} = -iZ_c \cot(k_p l/2). \tag{43}$$

There will also be an input reactance due to energy radiated and absorbed. However, numerically this will not be as large as the input reactance of (43), so it is neglected.

In Fig. 9, we plot the radiation resistance, input resistance, and input reactance as a function of l/λ, where λ is the free-space wavelength, assuming that $k_p = 100k$.

G. Discussion

Why is the radiation resistance so low, and why is it periodic in $k_p l/2$? The answer to that question is quite simple. To illustrate, we show schematically in Fig. 10 the current pattern on the antenna for three different values of $k_p l/2$.

The elements form what can be considered a phased array of current sources, but each element is out of phase with its nearest neighbor by 180°. The far-field electric field is the sum of the fields generated by each element. Because each element is out of phase, the fields from the individual elements cancel if there

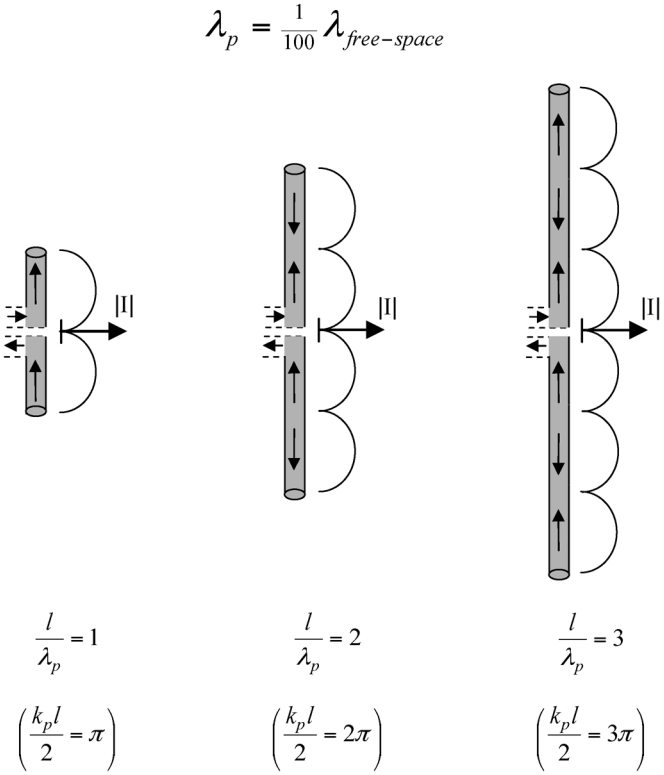

Fig. 10. Current distribution schematic for various lengths.

is an even number of elements. If there is an odd number of elements, all but one of the elements cancel.

This analysis can be carried even further. The analysis suggests that one can neglect all but the last odd element as radiating. This suggests that the antenna properties of a nanotube antenna whose length is an odd integer multiple of the λ_p is equivalent to the short thin wire antenna of length λ_p. Indeed, this is true quantitatively. The radiation resistance of an electrically short and physically short thin-wire antenna with constant current distribution is given by

$$R_{\rm rad} = 80\pi^2 \left(\frac{l}{\lambda}\right)^2. \tag{44}$$

Note that this is not exactly the case we have in mind, but it provides a first step in understanding how an electrically short current element radiates. Thus, its application in this case is semi-quantitative only but allows for improved physical insight as to why the radiation resistance is so low for nanotube antennas.

If we take $l = \lambda_p$, we get a radiation resistance of 0.08 Ω, which is almost exactly that predicted by our theory in Fig. 9. There is a factor of two difference because, for the last odd element, the current is not constant but periodic in space, whereas (44) for a thin-wire antenna assumes a constant spatial current distribution. The average current for a sinusoidal current distribution is $1/\sqrt{2}$ smaller than the max, thus accounting for the factor of two difference.

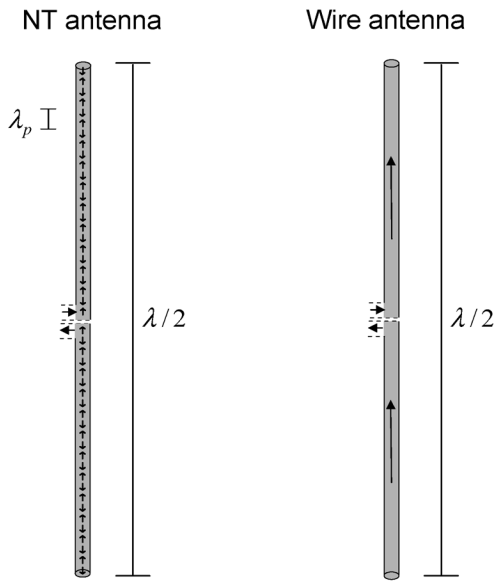

Fig. 11. Current distribution for nanotube versus wire antenna for length $\lambda/2$.

For longer antennas, where the length is comparable to the free-space wavelength, the elements of length λ_p are no longer close to each other compared to the free-space wavelength so that the situation is quantitatively more complicated. Equation (38) quantifies this situation. To emphasize this situation, in Fig. 11 we show a schematic comparison of the current distribution on a thin-wire antenna of length $\lambda/2$ versus the current distribution on a nanotube antenna of the same length.

This analysis suggests then, for a lossless nanotube, that making an antenna of length longer that one plasmon wavelength is not at all beneficial in terms of antenna properties. Since the plasmon wavelength is short, a nanotube antenna will, in the best case scenario, be only as good as a short thin-wire antenna, with length given by the plasmon wavelength, which is about 100 times smaller than the free-space wavelength. This, presumably, is a general property of slow-wave antennas, of which a nanotube is an extreme example.

VII. Radiation Properties Under Arbitrary Loss Conditions

A. Electric Field

In Section V, we solved for the current distribution under arbitrary loss conditions. We now use this current distribution to calculate the radiation properties. On substituting the general expression for the current [see (26)] into (28) for determining the far-field electric field, we have

$$E_\theta = i\eta \frac{ke^{-ikr}}{4\pi r} \sin\theta X \left\{ \int_{-l/2}^{0} \frac{V_0^+}{Z_C} \sinh\left[\gamma_p\left(\frac{l}{2}+z\right)\right] e^{ikz\cos\theta} dz + \int_{0}^{+l/2} \frac{V_0^+}{Z_C} \sinh\left[\gamma_p\left(\frac{l}{2}-z\right)\right] e^{ikz\cos\theta} dz \right\}. \tag{45}$$

Equation (45) can be evaluated, and the result is

$$E_\theta = -i\eta \frac{k}{\gamma_p} \frac{V_0^+}{Z_C} \frac{e^{-ikr}}{2\pi r} \sin\theta \frac{\cos\left(\frac{kl}{2}\cos\theta\right) - \cosh\left(\frac{\gamma_p l}{2}\right)}{1 + (k/\gamma_p)^2 \cos^2\theta}. \tag{46}$$

B. Poynting Vector and Radiation Intensity

The Poynting vector can be calculated from the electric field. Because γ_P and Z_C are complex, the result cannot easily be simplified but can be numerically calculated from (31). The radiation intensity can be numerically calculated from (33). The total radiated power can be determined by numerically integrating the radiation intensity over a sphere. The radiation resistance is not meaningful when there is intrinsic loss distributed along the antenna. The radiation pattern and directivity can also be numerically calculated.

C. Input Impedance

If we neglect the energy radiated, the input impedance is given by

$$Z_{\text{in}} = Z_c \coth(\gamma_p l/2). \tag{47}$$

This can also be numerically calculated.

VIII. Classification of Loss Regimes

Loss, or resistance, is an important parameter in nanotube antennas. There are two ways in which low loss can be defined. The first is that the frequency is high enough, and the loss low enough, so that the wave propagation on the two-nanotube transmission line is dispersion free. Mathematically, the requirement for this is

$$i\omega \mathcal{L}_K/4 \gg \mathcal{R}. \tag{48}$$

If one uses our recently measured value of 10 $k\Omega/\mu$m, the low-loss condition translates into a frequency requirement of

$$f > 400 \text{ GHz}. \tag{49}$$

However, if lower resistance tubes are grown this could be lower. For example, at cryogenic temperatures this requirement may be different. This issue is further discussed as follows. Under these low-loss conditions, the wave-vector is given by

$$\gamma_p \approx ik_p + \alpha. \tag{50}$$

The attenuation constant α is given by

$$\alpha = \frac{1}{2}\frac{\mathcal{R}}{Z_C}. \tag{51}$$

The physical interpretation of the attenuation coefficient is the length over which a propagating wave on the two-nanotube transmission line decays in amplitude by $1/e$. Additionally, under these conditions, (48), the characteristic impedance, is real and given by

$$Z_c \approx \sqrt{\frac{\mathcal{L}_K}{8\mathcal{C}_{\text{Total}}}}. \tag{52}$$

A second, stricter definition of low loss requires (48) be satisfied and, in addition, requires that the wave is not significantly attenuated over the length of the antenna. In mathematical terms, this can be expressed as

$$\frac{\alpha l}{2} \ll 1. \tag{53}$$

This second condition depends on the length of the nanotube.

IX. Low-Loss Calculations

In this section, we are interested in determining the effect of loss on antenna performance in the low-loss regime defined as both (48) and (53). We seek to find expressions for antenna efficiency correct to linear order in $\alpha L/2$.

For the following, we will divide the discussion into two cases: on-resonance, defined by $k_p l/2 = n\pi$, and off resonance, defined by $k_p l/2 \neq n\pi$.

A. Resonance Condition

Since the radiation resistance (which is already quite low) is highest on resonance, this case would be the most logical case for maximizing the antenna efficiency.

1) Resistive Losses: Neglecting radiation losses, what is the loss due to the ohmic dissipation? This depends on the resistance per length, antenna length, and frequency. We first calculate the input impedance (neglecting radiation resistance) on resonance. One can show that, on resonance, the real part of the input impedance (47) is given approximately by

$$Re(Z_{\text{in}}) \approx \frac{4Z_c^2}{\mathcal{R}l}. \tag{54}$$

This allows us to calculate the ohmic losses in the ultra-low loss condition. Specifically, for a given voltage at the terminals $V_{\text{terminals}}$, the power dissipated due to ohmic losses is given by

$$P_{\text{ohmic}} = \frac{1}{2}\frac{|V_{\text{terminals}}|^2}{Re(Z_{\text{in}})} = \frac{1}{2}|V_{\text{terminals}}|^2 \frac{\mathcal{R}l}{4Z_c^2}. \tag{55}$$

This will be used later.

Note that the imaginary part of the input impedance on resonance will be zero in the presence of any small amount of loss.

2) Radiative Losses: We seek an expression for the radiated power as a function of the voltage applied at the terminals, in order to compare with (55).

In the ultra-low loss case, the overall current distribution (27) is not significantly altered; therefore, the radiation resistance is not significantly altered. For the purposes of the radiation resistance, it is sufficient to assume that the current distributing is still approximately sinusoidal with amplitude I_0. If we make this assumption, then the power dissipated due to radiation is still related to the radiation resistance through (38), i.e.,

$$P_{\rm rad} = \frac{1}{2}|I_0|^2 R_r. \tag{56}$$

On resonance, the radiation resistance R_r is approximately equal to 0.03 Ω, as discussed in Section VI-D.

When there are resistive losses, the current distribution is slightly modified from being sinusoidal and the current at the terminals on resonance is given by $I_0 \sinh(\gamma_p l/2)$. On resonance, the current at the terminals can be approximated as

$$I_{\rm terminals} \approx 2I_0(\alpha l/2). \tag{57}$$

(The factor of two comes because the differential current at the terminals is two times the current on an individual tube.) Therefore, the radiated power can be written as

$$P_{\rm rad} = \frac{1}{2}|I_0|^2 R_r = \frac{1}{2}\frac{|I_{\rm terminals}|^2}{(\alpha l)^2} R_r. \tag{58}$$

This allows us to calculate the power dissipated as radiation. Specifically, for a given voltage at the terminals $V_{\rm terminals}$, the power dissipated due to radiation is given by

$$P_{\rm rad} = \frac{1}{2}\frac{|I_{\rm terminals}|^2}{(\alpha l)^2} R_r = \frac{1}{2}\left|\frac{V_{\rm terminals}}{Re(Z_{\rm in})}\right|^2 \frac{1}{(\alpha l)^2} R_r. \tag{59}$$

Based on (54), (59) can be expressed as

$$P_{\rm rad} = \frac{1}{2}|V_{\rm terminals}|^2 \frac{R_r}{Z_c^2}\frac{1}{4}. \tag{60}$$

This will be used later.

A comment about (60): This is interesting, because it shows that the radiated power does not depend on the resistance per length of the nanotube, in the low-loss limit. This is because the current distribution is assumed to be the same, regardless of the loss, which is approximately true. The radiated power depends only on the current distribution, so it does not change in this approximation. Only the current at the terminals changes and only by a small amount in the low-loss approximation.

3) Antenna Efficiency: We define the antenna efficiency as the ratio of the power dissipated in radiation to the total power dissipated (radiation and ohmic), i.e.,

$$\text{A.E.} \equiv \frac{P_{\rm rad}}{P_{\rm rad} + P_{\rm ohmic}}. \tag{61}$$

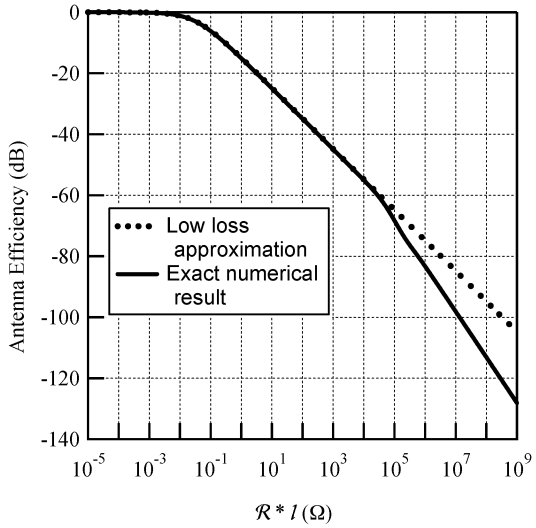

Fig. 12. Antenna efficiency versus $\mathcal{R}l$, assuming $l = 0.01\lambda$. Result is independent frequency or length, as long as equation is true.

Based on (60) and (55), this can be written as

$$\text{A.E.} = \frac{1}{1 + \mathcal{R}l/R_r} = \frac{1}{1 + \mathcal{R}l/0.03\,\Omega}. \tag{62}$$

This means that as soon as the nanotube dc resistance of length l exceeds 0.03 Ω, the resistive losses dominate. We plot in Fig. 12 the antenna efficiency as a function of Rl. Numerically, (62) is good to within 0.3 dB if $\mathcal{R}l$ is less than 10^4 Ω.

B. Off-Resonance Condition

In the off-resonance case, the discussion is similar. We want to determine the power dissipated due to radiation losses and ohmic losses, then calculate the antenna efficiency.

1) Resistive Losses: For small damping, off resonance, the real part of the input impedance (47) is given approximately by

$$Re(Z_{\rm in}) = Z_c \frac{\alpha l/2}{\sin^2(k_p l/2)} = \frac{\mathcal{R}l/4}{\sin^2(k_p l/2)}. \tag{63}$$

This allows us to calculate the ohmic losses in the ultra-low loss condition. For a given voltage at the terminals $V_{\rm terminals}$, the power dissipated due to ohmic losses is given by

$$P_{\rm ohmic} = \frac{1}{2}\frac{|V_{\rm terminals}|^2}{Re(Z_{\rm in})} = \frac{1}{2}|V_{\rm terminals}|^2 \frac{\sin^2(k_p l/2)}{\mathcal{R}l/4}. \tag{64}$$

2) Radiative Losses: Off resonance, the current at the terminals is not near a null, so the sinusoidal approximation can be used, i.e.,

$$I_{\rm terminals} = 2I_0 \sin(k_p l/2). \tag{65}$$

Combining this with (56), we find

$$P_{\rm rad} = \frac{1}{2}\frac{|I_{\rm terminals}|^2}{4\sin^2(k_p l/2)}R_r \tag{66}$$

$$= \frac{1}{2}\left|\frac{V_{\rm terminals}}{Re(Z_{\rm in})}\right|^2 \frac{1}{4\sin^2(k_p l/2)}R_r \tag{67}$$

$$= \frac{1}{2}|V_{\rm terminals}|^2 \sin^2(k_p l/2)\frac{4R_r}{(\mathcal{R}l)^2} \tag{68}$$

where we have used (63). This will be used later.

3) Antenna Efficiency: Based on (66) and (64), this can be written as

$$\text{A.E.} = \frac{1}{1+\mathcal{R}l/R_r}. \tag{69}$$

This is the same as the on-resonance condition. However, the radiation resistance R_r is frequency dependent and maximum on resonance. (See Fig. 9.) Therefore, the antenna efficiency will be maximum on resonance.

X. High-Loss Calculations

A. Loss Classification

We calculated the antenna efficiency in the low-loss case according to the criteria $\alpha l/2 < 1$. In this section, we seek to determine the antenna efficiency in the high-loss case according to the criteria $\alpha l/2 > 1$. If this criteria is met, and if the antenna is designed for microwave frequencies, then it is also going to be true that the system is in the high-loss case according to the condition $\omega\mathcal{L}_K < \mathcal{R}$. We elaborate.

If the antenna is designed for microwave frequencies, then the length will be of the order the plasmon wavelength at microwave frequencies, which is of order 100 μm. If this is the case, and it is true that $\alpha l/2 > 1$, then according to (51), the resistance per length will be at least of order 100 kΩ/μm, which is numerically larger than $\omega\mathcal{L}_K$ at microwave frequencies. Therefore, the high-loss calculations to be discussed in this section will be high loss in both senses of (48) and (53).

B. Qualitative Discussion

In the high-loss case, the current distribution is dramatically changed. Essentially, the only spatial region of the antenna which carries current is the region within α^{-1} of the terminals. By definition $\alpha l/2 > 1$, this is a small fraction of the entire antenna. This is seen clearly in Fig. 7, where we plot the current distribution for various loss values. For the highest values of $\mathcal{R}$, the current flows only near the terminals. It is dissipated as ohmic losses before reaching the end of the nanotubes, which are far away from the terminals on the scale of α^{-1}. Therefore, the radiated power and radiation efficiency will be significantly *lower* than the low-loss prediction (62).

C. Numerical Calculation

We have numerically evaluated the radiated power and ohmic dissipated power as a function of the $\mathcal{R}l$ product and then calculated the antenna efficiency as defined previously. The radiated power is calculated numerically by integrating the radiation intensity calculated from the electric field (45) over a sphere. The numerical integration was performed using a simple script in Mathematica. A length $l = 0.01\lambda$ was assumed for the calculations, which corresponds to the on-resonance case in the low-loss condition as discussed previously.

The ohmic losses are calculated numerically by calculating the power according to

$$P_{\rm ohmic} = \frac{1}{2}Re\left[V_{\rm terminals}I^*_{\rm terminals}\right] \tag{70}$$

and exploiting the input impedance given in (47) for the relationship between $V_{\rm terminals}$ and $I_{\rm terminals}$.

In Fig. 12, we plot the exact numerical solution for the antenna efficiency as a function of the parameter $\mathcal{R}l$. Interestingly, this curve is universal regardless of the frequency, the numerical value of $\mathcal{R}$, or the numerical value of l, as long as one assumes $l = 0.01\lambda$. Since we showed in the low-loss case that the antenna efficiency is maximized on resonance (which is true of $l = 0.01\lambda$), it is reasonable to assume antenna operation in the high-loss case would be for the same length.

D. Discussion

From Fig. 12, it can be seen that the low-loss approximation breaks down for an $\mathcal{R}l$ value of around 20 kΩ. For a nanotube antenna with a microwave resonance frequency, the length will be of order 100 μm. For this antenna, the low-loss approximation will break down at a numerical value of $\mathcal{R} \sim 100\ \Omega$. This value is about 100 times lower than our measured value of $\mathcal{R}$ of 10 kΩ/μm. Therefore, for available nanotube technology, the antenna will most likely operate in the high-loss region. However, since long nanotube devices are relatively new, this situation may be improved on in the future, if higher conductivity nanotubes can be grown. For realistic values of $\mathcal{R}$, the antenna efficiency is low. This is a drawback of nanotube antennas in the thin-wire geometry discussed in this paper. We return to this issue the following.

XI. Impedance Matching

We wish now to discuss the input impedance and the issue of impedance matching.

A. Numerical Evaluation of Input Impedance

We found the antenna efficiency is maximized in the resonant case, which is therefore the most likely regime of operation. On this resonance, the imaginary part of the input impedance is *zero*. Therefore, one only has to deal with the real input impedance. We plot in Fig. 13 the input impedance, calculated from (47), as a function of $\mathcal{R}l$. We have again assumed that $l = 0.01\lambda$.

In the low-loss case, the input impedance diverges, because the resonance causes a null in the current at the antenna terminals. (See Fig. 7.) As the loss increases, the current at the terminals increases, thus decreasing the input impedance. When the input impedance becomes numerically equal to the characteristic impedance, this corresponds to the condition $\alpha l/2 \sim 1$.

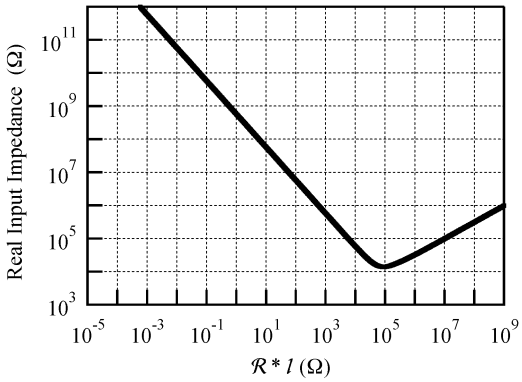

Fig. 13. Real input impedance at antenna terminals versus $\mathcal{R}l$, assuming $l = 0.01\lambda$. Result is independent frequency or length, as long as equation is true.

Above this value, the input impedance increases again, this time due to the severe ohmic losses. Interestingly, this curve is also a universal curve regardless of the frequency, the numerical value of $\mathcal{R}$, or the numerical value of l, as long as one assumes $l = 0.01\lambda$.

Off resonance, the imaginary impedance will be very large and frequency dependent, making impedance matching more complicated.

B. Natural Transformer From Free Space to Quantum Impedance

The input impedance is high, of the order or larger than the resistance quantum of 25 kΩ. This is no surprise, because in our model the antenna is fed with a high-impedance two-nanotube transmission line. Thus, the nanotube antenna on resonance can be viewed as a *natural quantum transformer* that transforms the characteristic impedance of free space (120π Ω) up to the quantum impedance (h/e^2), assuming one is on resonance. Because most nanodevices and circuits are inherently high impedance, this is a desired property of the system.

XII. Discussion

A. Loss and Efficiency

The fact that a nanotube current distribution has a different wavelength than the free-space wavelength restricts its properties, in the best case, to be equivalent to those of a short thin-wire antenna. This means the radiation resistance is low and causes any small ohmic resistance to reduce the overall antenna efficiency significantly. For current nanotube technology, this is a big challenge.

For impedance matching to quantum devices, it appears the optimum $\mathcal{R}l$ product is about 10 kΩ, which translates into a resistance per length of about 10 Ω/μm. This may be achievable in the near term at room temperature for nanotube antennas and is likely achievable at cryogenic temperatures. According to our calculations, this would correspond to an antenna efficiency of about −60 dB. Clearly, this is not suitable for long-range wireless communications systems. However, it is generally a large unsolved problem to make electrical contact to the nanoworld and even more difficult to transfer more abstract information from the macroworld to the nanoworld. In this case, a wireless link from an integrated nanosystem to the macroscopic world may still be advantageous over lithographic interconnects from a *systems* point of view, in spite of the somewhat low antenna efficiency. This problem of low-efficiency contact to the nanoworld is not unique to wireless interconnects. With dc contact to nanodevices, the contact resistance is typically high and is a complicated physical phenomenon. From this perspective, wireless connections offer a much "cleaner" physical system, with less ambiguities such as Schottky barriers, quantum contact resistances, and similar issues currently being heavily investigated the field of nanoelectronic devices.

B. Transition From Nanoantenna to Thin-Wire Antenna

A question which naturally arises in this context is: How thin does a wire have to be for its behavior as an antenna to be different than a regular thin-wire antenna? This can be rephrased: at what diameter is the kinetic inductance comparable to the magnetic inductance? The magnetic inductance is only weakly dependent on the diameter, and is about 1 pH/μm. A rough estimate for how the kinetic inductance scales with length comes from observing that the kinetic inductance per unit length is crudely m/ne^2, where n is the number of electrons per length. If one assumes metallic systems with one electron per atom, and atoms of size 1 angstrom, then for a diameter of d, the number of electrons per meter along the wire is approximately $1/d^2$, with d in angstroms. Therefore, the kinetic inductance is approximately $(1/d^2) \times 10^{-11}$ H/m. Equating this with the magnetic inductance and solving for d, we find that a value of $d = 100$ nm is the critical diameter demarcating the boundary between nanoantenna, where kinetic inductance dominates, and thin-wire antenna, where magnetic inductance dominates. There is clearly plenty of room to engineer antenna performance in the intermediate regime. This is an interesting topic for future study.

C. Assumptions

There are a number of unproven assumptions in this paper. First, we argued that the effective circuit model of a two-nanotube transmission line includes kinetic inductance and quantum capacitance as dominant circuit elements. Second, we argued that the radiation does not affect the current distribution on the nanotube significantly. Third, we argued that the radiation *reactance* is small compared to the kinetic inductance, but we did not explicitly calculate the radiation reactance. These arguments, while reasonable, should be put on more rigorous grounds through self-consistent calculations that include the full quantum properties of electrons in coupled two-nanotube systems and their interaction with microwave radiation. Our work should be viewed as an engineer's attempt to simplify a complicated physical system down to its most important basic elements in order to provide simplified approximations for antenna performance.

D. Alternative Geometries

In our calculations, we have considered the simplest antenna geometry, that of a thin-wire antenna. In this case, the radiation resistance turns out to be very low, so that minimizing ohmic resistance is a critical issue. In other words, for resistive nanotubes, the antenna efficiency is low. However, our work is only the first step in the design of nanoantennas. For example, there

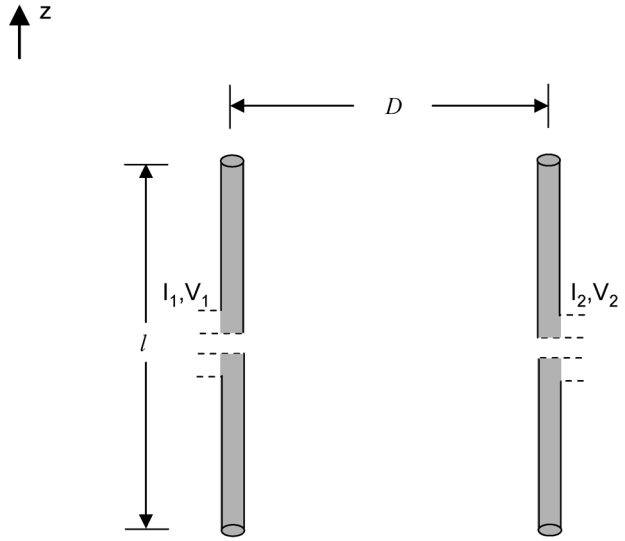

Fig. 14. Side-by-side antenna geometry assumed.

may be other, alternative geometries that are more suited to particular properties of nanotubes, such as the high kinetic inductance and high resistance. This remains an open question for future work.

E. Future Work

Our work is really only a baby step in the field of the integration of wireless technology with nanotechnology. The next logical question is, *to what do you connect to the terminals of the antenna?* This is related to the nascent field of nanoelectronics architecture, which has many issues remaining to be solved. In this context, our work in this paper provides initial steps in understanding the antenna properties of nanotubes and nanowires, which will be needed for the future architecture work.

XIII. Near-Field Coupling

Typically, an antenna is intended to be used to communicate between distant physical objects: the receiver and transmitter are usually physically separated by many wavelengths. Thus, for the previous calculations, we have focused on the far-field radiation properties of nanotubes.

Due to the high resistance of a nanotube, the far-field efficiency for currently grown single walled carbon nanotubes is low. Therefore, in this section we consider the near-field properties. On-chip ac coupling from one nanotube to another may be a more feasible near term prospect. In addition, our calculations in this section should have important applications in the future use of nanotubes as high-frequency interconnects in *integrated nanosystems*.

A. Model Geometry

In Fig. 14, we show the model geometry we consider. In the first section of this paper, we considered a single nanotube antenna without any other conductors nearby and calculated the radiation pattern in the far field.

In case there are nearby objects, say several other antennas, the input impedance of a nanotube antenna can still be represented by a two-terminal network. However, the value of this input impedance is determined not only by the self-impedance of the antenna but also by he mutual impedances between it and the other antennas and the currents flowing in them [45].

In order to solve this problem, we use an induced EMF method to calculate the impedance matrix that relates the currents and voltages at each antenna terminal. This matrix is given by

$$V_1 = I_1 Z_{11} + I_2 Z_{12} \tag{71}$$
$$V_2 = I_2 Z_{21} + I_2 Z_{22} \tag{72}$$

where V_1 and V_2 are the voltages at the terminals of antenna 1 and 2, respectively, and I_1 and I_2 are the currents at the terminals of antennas 1 and 2, respectively. In this paper, we assume both antennas are identical in geometry. In this case, $Z_{11} = Z_{22}$, and this is the input impedance of the antenna calculated previously for the far-field case, i.e., (47). Additionally, reciprocity implies that $Z_{12} = Z_{21}$. Therefore, to calculate the mutual impedance Z_{12} between the two antennas, we need only to determine Z_{12}. This is discussed next. For this paper, we discuss the mutual impedance in the no-loss case (i.e., we neglect the ohmic resistance of the nanotubes).

B. Induced EMF

In this section, we use the standard technique for calculating the mutual impedance between two dipole antennas. In standard antenna theory, the reciprocity theorem is used to prove that Z_{21} is given by [44]

$$Z_{21} = -\frac{1}{I_{1i} I_{2i}} \int_{-l/2}^{l/2} E_{z21}(z) I_2(z) dz \tag{73}$$

where I_{1i} is the current at the terminals of antenna 1 (and similarly for antenna 2), $I_2(z)$ the current distribution on antenna 2, and $E_{21}(z)$ the electric field produced by antenna 1 at the surface of antenna 2. In deriving this equation it is usually assumed that the tangential component of the electric field at the surface of both antennas is zero. In the case of a nanotube antenna, this is not necessarily true. For the purposes of this paper, we conjecture that (73) describes the mutual impedance even when the boundary condition at the surface of the antenna is different than a perfect conductor.

C. Exact Field of Nanotube Antenna

In this section, we calculate the exact field of a nanotube antenna, assuming a current distribution given by (27). We first calculate the vector potential as [44]

$$A_z(x,y,z,t) = \frac{\mu I_0}{4\pi} \int_{-l/2}^{l/2} \frac{\sin\left[k_p\left(l/2 - |z'|\right)\right] e^{-ikR}}{R} dz' \tag{74}$$

where $R = [x^2 + y^2 + (z - z')^2]^{1/2}$. In Appendix III, we perform this integral and determine the exact electric field for a nanotube

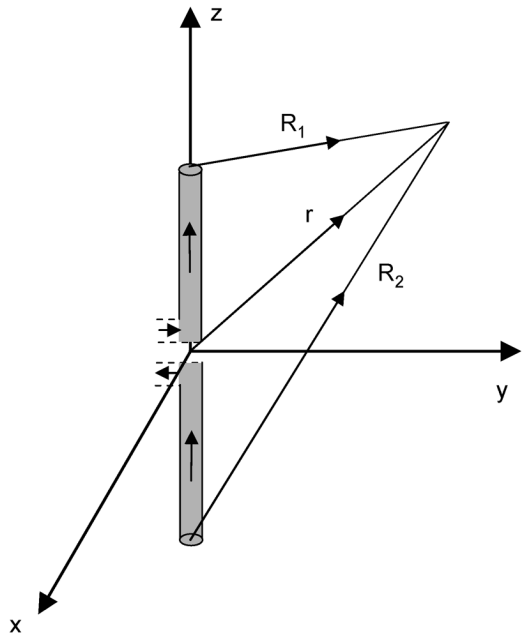

Fig. 15. Coordinate system for exact electric field calculation.

antenna, valid for both the near field and the far field. We find (using the coordinates as shown in Fig. 15)

$$E_z = -j\frac{\eta I_0}{4\pi}\left[\frac{e^{-ikR_1}}{R_1} + \frac{e^{-ikR_2}}{R_2} - 2\cos\left(\frac{k_p l}{2}\right)\frac{e^{-ikr}}{r}\right]. \tag{75}$$

D. Mutual Impedance

Once the exact electric field produced by an individual nanotube is known, the mutual impedance can be calculated based on (73)

$$Z_{21} = i\frac{30}{\sin^2(k_p l/2)}\int_{-l/2}^{l/2}\sin\left[k_p\left(l/2 - |z|\right)\right] \tag{76}$$

$$X\left[\frac{e^{-ikR_1}}{R_1} + \frac{e^{-ikR_2}}{R_2} - 2\cos\left(\frac{k_p l}{2}\right)\frac{e^{-ikr}}{r}\right]dz. \tag{77}$$

E. Numerical Evaluation of Mutual Impedance

In this section, we consider the numerical evaluation of (77). For the purposes of this paper, we will consider two nanotubes with spacing that is of the order the plasmon wavelength. Since this length is approximately 100 times smaller than the free-space wavelength, we can approximate the exponentials with their Taylor expansion. Since we are interested in power coupling, we focus on the real part of Z_{21}. We also will assume, for simplicity, that the overall antenna length is an integral number of odd half plasmon wavelengths so that the third term in the integrand vanishes. In this case, the only term left to integrate is a sine term, which can be done analytically. The results are given as follows:

$$Re(Z_{21}) \approx 120\left(\frac{k}{k_p}\right) \tag{78}$$

$$\approx 1.2\,\Omega \tag{79}$$

where we have assumed $k_p l = \pi$. Note that in this limit (nanotubes much closer to each other than the free-space wavelength), the real mutual impedance is independent of distance.

F. Mutual Impedance: Discussion

The goal of this section was to calculate the mutual impedance to determine whether nanotubes could act as better antennas when used in the near field rather than the far field. The answer is clearly yes. The physical interpretation of the mutual impedance is that if it is larger than the self-impedance, there is significant coupling between the antennas. Since the self-impedance (calculated previously) is typically of order $0.02\ \Omega$, the mutual impedance is much larger.

We have not yet considered the effect of ohmic losses quantitatively on the near-field coupling. However, because the mutual impedance is larger than the self-impedance, it will be less effected by ohmic losses.

Although we only we considered numerically the case where the nanotubes were closer together than the free-space wavelength, the general procedure described could be used for arbitrary antenna spacing and orientation.

XIV. Integral Equation for Antenna Current

In the previous sections, we *assumed* the form for the current distribution was given by (26). However, this was only argued on the basis of intuition and not rigorously proved. In this section, we derive an integral equation which would allow for a full numerical calculation of the current distribution on a nanotube antenna.

Such an integral equation approach allows one to use the "Maxwellian" approach and treat the problem numerically. The advantage of such an approach is its exactness and the ability to treat the detailed shape of the flare at the terminal regions of the antenna. The disadvantage is the extra overhead required to set up the numerical processing and also (more importantly) the lack of physical insight. One risks losing this insight by programming Maxwell's equations into a computer and reading out the result without critical evaluation.

A. Boundary Conditions: Perfect Metal

The boundary conditions for the electric field $\vec{E}$ are that the tangential component of the electric field is continuous. In a perfect metal, the electric field is zero inside the metal, and all the currents flow on the surface (at ac). This gives rise to the boundary condition that the electric field tangential to the metal is zero at the surface of the metal. This approximation gives numerically correct results (radiation resistance and reactance, current distribution, and radiation pattern) for most antennas.

B. Finite Conductivity Metal: Skin Depth

For metals with finite conductivity, there is some penetration of the electric field into the conductor, the so-called skin depth. Typically, the skin depth is of order 1 μm. Because this is typically much larger than the diameter of a classical thin-wire antenna, it is numerically approximately correct to assume that all the currents flow on the surface of the conductor.

The skin-effect also gives rise to a small surface resistance and surface inductance. The physical origin of the surface resistance is simple: The electric field penetrates into the conductor; there is some current flowing parallel to the electric field; hence, there is some power dissipated, i.e., resistance. The physical origin of the surface inductance is also simple: There is some magnetic field inside the metal which gives rise to stored (magnetic) energy along the surface of the metal. This stored energy is equated with $LI^2/2$, i.e., an inductance. Numerically, since these resistances and inductances are typically small, they are usually approximated as zero, at least as far as antenna theory is concerned.

C. Boundary Conditions: Nanoantenna

The boundary conditions for a nanotube antenna are quite distinct. Although a full quantum calculation would be necessary to correctly determine the boundary conditions [46]–[53], for this paper we provide an estimate only. In this paper, we model the electrons as confined in one dimension. This means they cannot move in the transverse direction, but only along the nanotube axis. To elaborate, in a classical diffusive wire, electrons are free to diffuse in all three directions. This gives rise, at ac, to the exclusion of electric fields (and currents) inside the conductor and penetration of the electric fields and currents within one skin-depth (typically a few micrometers) of the surface. Since the diameter of a nanotube (a few nanometers) is much less than the skin depth, this model is clearly not appropriate. In this paper, we neglect the fact that there is a hollow "core" inside the nanotube and instead treat the current as uniformly distributed over the cross-sectional area of the nanotube. This is not physically the actual situation, but we argue it should give approximately correct results for antenna properties.

A second question is where the actual boundary is between the surface of the nanotube and free space. Since we consider a system with atomic dimensions, the distributed nature of the electronic wave function makes this question difficult to answer exactly. For the purposes of this paper, we will assume there is a boundary that is of the order of the diameter of the nanotube between "conductor" and free space.

These considerations, of course, dramatically change the boundary conditions compared to a classical thin-wire antenna. If the nanotube impedance parallel to its axis were only resistive, we would have a simple linear relationship between the electric field component along the nanotube and the current flow along the nanotube. However, as we have argued previously, there is also a large inductance component of the nanotube impedance, which also needs to be taken into account. On this basis, we argue that the boundary condition for the electric field on the surface of the nanotube is given by

$$E_{\|} = (\mathcal{R} + i\omega\mathcal{L}_K/4)I. \tag{80}$$

Here, I is the current flowing along the nanotube, which is position dependent, and $\mathcal{R}$ is the resistance per unit length (assumed numerically equal to the dc resistance per unit length) and $\mathcal{L}_K/4$ the kinetic inductance per unit length, with the factor of four due to band structure and spin degeneracy, as explained.

The distributed resistance in (80) can be thought of as the analog of the surface resistance for a classical thin-wire antenna. However, the kinetic inductance is not analogous to the surface inductance of a classical thin-wire antenna. For a classical thin-wire antenna, it is usually assumed that the conductivity σ, defined through the relationship $J = \sigma E$, is real and independent of frequency. However, the kinetic inductance in this paper actually refers to a situation where the conductivity has a real and imaginary component, and the imaginary impedance is given by $i\omega\mathcal{L}_K/4$.

In this section, we have neglected the quantum capacitance for two reasons. First, it is not immediately clear how to incorporate it into the relationship between the electric field and the electrochemical potential; second, it would not have a large quantitative effect on the conclusions.

D. Integral Equation

In this section, we follow the work of Hallen as notated in Kraus [54]. The electric field $\vec{E}$ and the vector potential $\vec{A}$ are related by

$$\vec{E} = -i\frac{c^2}{\omega}\vec{\nabla}(\vec{\nabla}\cdot\vec{A}) - i\omega\vec{A}. \tag{81}$$

The tangential component of E will lie in the z direction, assuming the same coordinate system as in Fig. 6; the current is also in the z direction. Hence, the vector potential $\vec{A}$ has only a z component so that (81) becomes

$$E_z = -i\frac{\omega}{k^2}\left(\frac{\partial^2 A_z}{\partial z^2} + k^2 A_z\right). \tag{82}$$

By enforcing the boundary condition that the tangential component of the electric field just outside the surface of the nanotube (82) is equal to the tangential component of the electric field inside the nanotube (80), we find the following relationship between A_z and I:

$$\frac{\partial^2 A_z}{\partial z^2} + \beta^2 A_z = \frac{k^2}{\omega}(\mathcal{R} + i\omega\mathcal{L}_K/4)I. \tag{83}$$

The solution of (83) can be written in integral form as

$$A_z = C_1\cos(kz) + C_2\sin(kz) + \frac{i(\mathcal{R} + i\omega\mathcal{L}_K/4)}{c}\int_0^z I(s)\sin\left(k(z-s)\right)ds. \tag{84}$$

We can also express the vector potential in terms of the current on the antenna as

$$A_z = \frac{\mu e^{i\omega t}}{4\pi} \int_{-l/2}^{l/2} \frac{I_{z1} e^{-ikr}}{r} dz_1 \tag{85}$$

where $r = [\rho^2 + (z - z_1)^2]^{1/2}$, and z_1 is a point on the surface of the nanotube. By equating (85) with (84), we find

$$\frac{\mu}{4\pi} \int_{-l/2}^{l/2} \frac{I_{z1} e^{-ikr}}{r} dz_1 = C_1 \cos(kz) + \frac{V_T}{2} \sin(k|z|) + \frac{i(\mathcal{R} + i\omega \mathcal{L}_K/4)}{c} \int_0^z I(s) \sin(k(z-s))\, ds. \tag{86}$$

This equation is similar to Hallen's integral equation, with the exception of the kinetic inductance and distributed resistance term.

E. Discussion

Although we have not carried out the numerical solution of (86), we claim that if it was carried out, the current distribution would be approximately given by (26). If this hypothesis is wrong, then so are the conclusions of this paper. (Note that after this paper was submitted, a numerical approach appeared in print which seems to confirm this hypothesis [55].) The reasoning for this argument is simple. In the case of a thin-wire antenna, the current distribution for the parallel two-wire transmission line (sinusoidal) is approximately the same as for the thin-wire antenna. By analogy, we expect that the current distribution for the nanotube antenna is approximately the same as for the two-nanotube transmission line system. This has already been indicated schematically in Fig. 5.

In the case of thin-wire antennas, there is an important difference between the exact solution and the approximate (sinusoidal) solution for the current distribution: When there is an antinode in the current at the terminals of the antenna, the current is zero; hence, the input impedance diverges. In our approximate theory for the nanoantenna, we also predict this divergence in the input resistance [see (42)]. Thus, while our analytical theory provides estimates of nanotube antenna performance, more quantitative work will require a numerical solution of (86).

XV. Conclusion

Simply speaking, one cannot think of a nanotube antenna in the same way as a thin-wire antenna because of the excess inductance of the order 10^4 time of the inductance of a thin-wire antenna. This translates into performance predictions which are substantially different than thin-wire antennas, essentially because the wavelength of the current excitation is 100 times smaller than the wavelength of the far-field radiation, a unique situation.

An advantage of nanotube antennas is that the nanotube can serve as an excellent impedance matching circuit to get from free space to high-impedance devices. A disadvantage, for current growth technology, is the low efficiency. With the nanotubes we are able to grow in our lab, we can achieve a predicted antenna efficiency of -90 dB.

With future, higher mobility nanotubes, better performance would be possible; although, prospects of approaching efficiencies of the order of unity seem dim with the simple thin-wire geometry considered in this paper. (For this, alternative geometries may be required.) Doing so will require nanotubes with ballistic transport over 100 s of micrometers. That is maybe not totally unrealistic. After almost 30 years of research on molecular beam epitaxy (MBE) growth, it is now possible in 2DEGs at cryogenic temperatures to achieve ballistic transport over 100 s of micrometers. The reduced phase space for scattering in carbon nanotubes (CNTs) makes it possible to have much higher mobilities than 2-D systems, so it is conceivable to achieve. In that case, and for more realistic lossy cases, our theory provides quantitative predictions for expected nanowire and nanotube antenna performance.

In an interesting historical aside, we have come almost completely full circle. Over 50 years ago, Hallen found one of the only analytical solutions to the current distribution on a radiating system. This solution was exact only in the limit that the length/diameter ratio was infinite. Since that time, most antenna work has focused on numerical methods to treat various geometries which could not be solved analytically. Now, with the advent of centimeter-long carbon nanotubes, mankind has found a technique to fabricate conducting wires with unprecedented aspect ratios of order 10^7. It is somewhat ironic that the conclusions of this paper are that the only analytical theory available for antenna properties actually does not apply at all in the small-diameter limit assumed. When the diameter is a nanometer, the antenna behavior is quite distinct.

Appendix I

In Fig. 16, we plot ξ assuming $k_p = 100k$.

Appendix II

In Fig. 17, we plot the calculated directivity as a function of $l/\lambda = kl/2\pi = 0.01 k_p l/2\pi$.

Appendix III

In this appendix, we calculate the exact electric field from a carbon nanotube antenna. This discussion follows very closely that of Balanis [44]. We calculate the magnetic field using

$$\vec{H} = -\hat{\phi} \frac{1}{\mu} \frac{\partial A_z}{\partial \rho}. \tag{87}$$

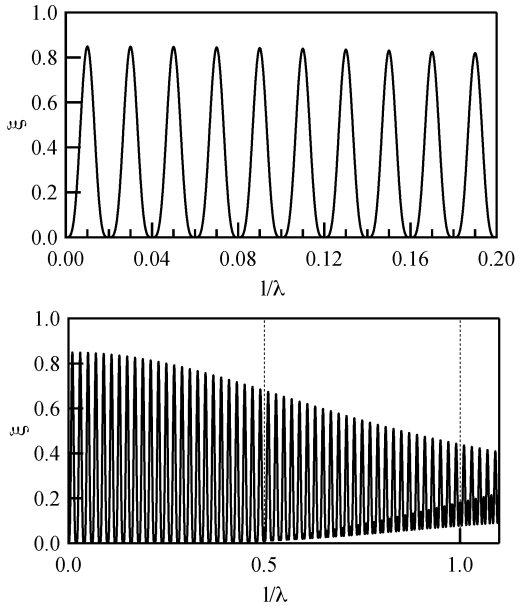

Fig. 16. Plot of ξ. x axis is $l/\lambda = kl/2\pi = 0.01k_pl/2\pi$.

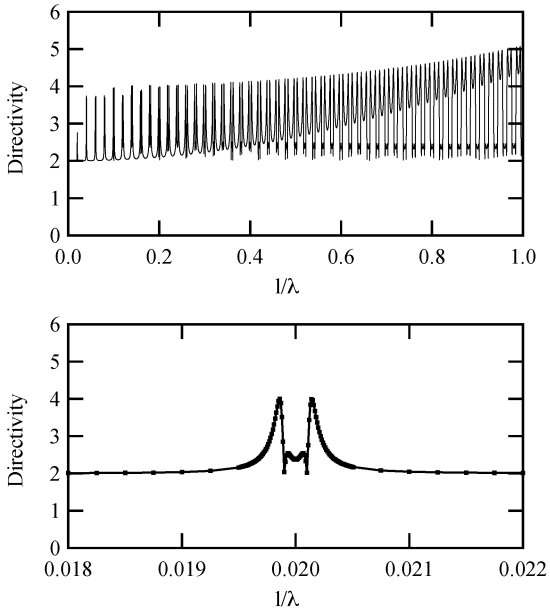

Fig. 17. Directivity. x axis is $l/\lambda = kl/2\pi = 0.01k_pl/2\pi$.

Choosing $\phi = \pi/2$ for convenience (without loss of generality) and transferring to cylindrical coordinates, we have

$$\vec{H} = -\hat{\phi}\frac{I_0}{4\pi}\frac{\partial}{\partial y}\left\{\int_{-l/2}^{0}\frac{\sin\left[k_p(l/2+z')\right]e^{-ikR}}{R}dz' + \int_{0}^{l/2}\frac{\sin\left[k_p(l/2-z')\right]e^{-ikR}}{R}dz'\right\}. \quad (88)$$

Expanding the sin term with Euler's relation we find

$$\begin{aligned} H_\phi = -\frac{I_0}{8\pi i}\Bigg\{ & e^{ik_pl/2}\int_{-l/2}^{0}\frac{\partial}{\partial y}\left[\frac{e^{-i(kR-k_pz')}}{R}\right]dz' \\ & - e^{-ik_pl/2}\int_{-l/2}^{0}\frac{\partial}{\partial y}\left[\frac{e^{-i(kR+k_pz')}}{R}\right]dz' \\ & + e^{ik_pl/2}\int_{0}^{l/2}\frac{\partial}{\partial y}\left[\frac{e^{-i(kR+k_pz')}}{R}\right]dz' \\ & - e^{-ik_pl/2}\int_{0}^{l/2}\frac{\partial}{\partial y}\left[\frac{e^{-i(kR-k_pz')}}{R}\right]dz'\Bigg\}. \end{aligned} \quad (89)$$

The third term within the brackets can be written as

$$\begin{aligned} & e^{ik_pl/2}\int_{0}^{l/2}\frac{\partial}{\partial y}\left[\frac{e^{-i(kR+k_pz')}}{R}\right]dz' \\ & = e^{ik_pl/2}\int_{0}^{l/2}\left\{\frac{1}{R}\frac{\partial}{\partial y}\left[e^{-i(kR+k_pz')}\right] + e^{-i(kR+k_pz')}\frac{\partial}{\partial y}\left(\frac{1}{R}\right)\right\}dz'. \end{aligned} \quad (90)$$

The two terms can be expanded to yield

$$\begin{aligned} \frac{\partial}{\partial y}\left[e^{-i(kR+k_pz')}\right] &= \frac{\partial}{\partial y}\left[e^{-i\left(k\sqrt{x^2+y^2+(z-z')^2}+k_pz'\right)}\right] \\ &= -ik\frac{y}{R}e^{-i(kR+k_pz')} \end{aligned} \quad (91)$$

$$\begin{aligned} \frac{\partial}{\partial y}\left(\frac{1}{R}\right) &= \frac{\partial}{\partial y}\left\{\left[x^2+y^2+(z-z')^2\right]^{-1/2}\right\} \\ &= -\frac{y}{R^3}. \end{aligned} \quad (92)$$

Thus, the previous equation can be expressed as

$$\begin{aligned} & e^{ik_pl/2}\int_{0}^{l/2}\frac{\partial}{\partial y}\left[\frac{e^{-i(kR+k_pz')}}{R}\right]dz' \\ & = ye^{ik_pl/2}\int_{0}^{l/2}\left[-jk\frac{e^{-i(kR+k_pz')}}{R^2} - \frac{e^{-i(kR+k_pz')}}{R^3}\right]dz'. \end{aligned} \quad (93)$$

Consider now the differential of

$$\begin{aligned} & d\left[\frac{e^{-i(kR+k_pz')}}{R(R+z'-z)}\right] \\ & = d\left[R^{-1}(R+z'-z)^{-1}e^{-i(kR+k_pz')}\right] \\ & = e^{-j(kR+k_pz')}\left[\frac{dR^{-1}}{(R+z'-z)} + \frac{d(R+z'-z)^{-1}}{R} - i\frac{d(kR+k_pz')}{R(R+z'-z)}\right]. \end{aligned} \quad (94)$$

Each term can be written as

$$\begin{aligned}\frac{dR^{-1}}{(R+z'-z)} &= \left[\frac{(z-z')}{R^3(R+z'-))}\right]dz' \\ \frac{d(R+z'-z)^{-1}}{R} &= -\left[\frac{(R+z'-z)^{-2}d(R+z'-z)}{R}\right] \\ &= -\left[\frac{1}{R^2(R+z'-z)}\right]dz' \\ &\quad -i\left[\frac{d(kR+k_pz')}{R(R+z'-z)}\right] \\ &= -ik\left(\frac{1}{R^2}\right)dz'. \end{aligned} \tag{95}$$

Thus, we have

$$d\left[\frac{e^{-i(kR+k_pz')}}{R(R+z'-z)}\right] = e^{-i(kR+k_pz')}\left[-\frac{1}{R^3}-ik\frac{1}{R^2}\right]dz'. \tag{96}$$

Using this, we can express

$$\begin{aligned} & e^{ik_pl/2}\int_0^{l/2}\frac{\partial}{\partial y}\left[\frac{e^{-i(kR+k_pz')}}{R}\right]dz' \\ &= ye^{ik_pl/2}\int_0^{l/2} d\left[\frac{e^{-i(kR+k_pz')}}{R(R+z'-z)}\right] \\ &= ye^{ik_pl/2}\left[\frac{e^{-i(kR_1+k_pl/2)}}{R_1(R_1+l/2-z)}-\frac{e^{-ikr}}{r(r-z)}\right] \end{aligned} \tag{97}$$

where

$$\begin{aligned} R_1 &= \sqrt{x^2+y^2+(z-l/2)^2} \\ &= \sqrt{y^2+(z-l/2)^2} \end{aligned} \tag{98}$$

$$\begin{aligned} r &= \sqrt{x^2+y^2+z^2} \\ &= \sqrt{y^2+z^2}. \end{aligned} \tag{99}$$

Using these, we can rewrite the previous equation as

$$\begin{aligned} & e^{ik_pl/2}\int_0^{l/2}\frac{\partial}{\partial y}\left[\frac{e^{-i(kR+k_pz')}}{R}\right]dz' \\ &= \frac{e^{ik_pl/2}}{y}\left[\left(1-\frac{l/2-z}{R_1}\right)e^{-i(kR_1+k_pl/2)}\right. \\ &\qquad \left.-\left(1+\frac{z}{r}\right)e^{-ikr}\right]. \end{aligned} \tag{100}$$

Using similar arguments, one finds

$$\begin{aligned} & e^{ik_pl/2}\int_{-l/2}^{0}\frac{\partial}{\partial y}\left[\frac{e^{-i(kR-k_pz')}}{R}\right]dz' \\ &= \frac{e^{ik_pl/2}}{y}\left[\left(1-\frac{l/2+z}{R_2}\right)e^{-i(kR_2+k_pl/2)}\right. \\ &\qquad \left.-\left(1-\frac{z}{r}\right)e^{-ikr}\right] \end{aligned} \tag{101}$$

$$\begin{aligned} & -e^{-ik_pl/2}\int_{-l/2}^{0}\frac{\partial}{\partial y}\left[\frac{e^{-i(kR+k_pz')}}{R}\right]dz' \\ &= \frac{e^{-ik_pl/2}}{y}\left[\left(1+\frac{l/2+z}{R_2}\right)e^{-i(kR_2-k_pl/2)}\right. \\ &\qquad \left.-\left(1+\frac{z}{r}\right)e^{-ikr}\right] \end{aligned} \tag{102}$$

$$\begin{aligned} & -e^{-ik_pl/2}\int_{0}^{l/2}\frac{\partial}{\partial y}\left[\frac{e^{-i(kR-k_pz')}}{R}\right]dz' \\ &= \frac{e^{-ik_pl/2}}{y}\left[\left(1+\frac{l/2-z}{R_1}\right)e^{-i(kR_1-k_pl/2)}\right. \\ &\qquad \left.-\left(1-\frac{z}{r}\right)e^{-ikr}\right]. \end{aligned} \tag{103}$$

Using these, we find

$$H_\phi = -\frac{I_0}{4\pi i}\frac{1}{y}\left[e^{-ikR_1}+e^{-ikR_2}-2\cos\left(\frac{k_pl}{2}\right)e^{-ikr}\right]. \tag{104}$$

The electric field can be determined from the magnetic field using one of Maxwell's equations

$$\vec{E} = \frac{1}{i\omega\epsilon}\vec{\nabla}\times\vec{H} \tag{105}$$

which in the y-z plane becomes for E_z

$$E_z = \frac{1}{i\omega\epsilon}\frac{1}{y}\frac{\partial}{\partial y}(yH_\phi). \tag{106}$$

Using this, and the previous expression for the magnetic field, we find

$$E_z = -j\frac{\eta I_0}{4\pi}\left[\frac{e^{-ikR_1}}{R_1}+\frac{e^{-ikR_2}}{R_2}-2\cos\left(\frac{k_pl}{2}\right)\frac{e^{-ikr}}{r}\right]. \tag{107}$$

REFERENCES

[1] S. Li, Z. Yu, S. F. Yen, W. C. Tang, and P. J. Burke, "Carbon nanotube transistor operation at 2.6 GHz," *Nano Lett.*, vol. 4, no. 4, pp. 753–756, 2004.

[2] Z. Yu and P. J. Burke, "Microwave transport in metallic single-walled carbon nanotubes," *Nano Lett.*, vol. 5, no. 7, pp. 1403–1406, 2005.

[3] J. Appenzeller and D. J. Frank, "Frequency dependent characterization of transport properties in carbon nanotube transistors," *Appl. Phys. Lett.*, vol. 84, no. 10, pp. 1771–1773, 2004.

[4] S. Rosenblatt, H. Lin, V. Sazonova, S. Tiwari, and P. McEuen, "Mixing at 50 GHz using a single-walled carbon nanotube transistor," *Appl. Phys. Lett.*, vol. 87, p. 15311, 2005.

[5] P. J. Burke, "An RF circuit model for carbon nanotubes," *IEEE Trans. Nanotechnol.*, vol. 2, no. 1, pp. 55–58, Jan. 2003.

[6] ——, "Luttinger liquid theory as a model of the gigahertz electrical properties of carbon nanotubes," *IEEE Trans. Nanotechnol.*, vol. 1, no. 3, pp. 129–144, May 2002.

[7] ——, "Luttinger liquid theory as a model of the gigahertz electrical properties of carbon nanotubes (erratum)," *IEEE Trans. Nanotechnol.*, vol. 3, no. 2, pp. 331–331, Mar. 2004.

[8] ——, "An RF circuit model for carbon nanotubes (erratum)," *IEEE Trans. Nanotechnol.*, vol. 3, no. 2, pp. 331–331, Mar. 2004.

[9] Z. Yu, S. Li, and P. J. Burke, "Synthesis of aligned arrays of millimeter long, straight single walled carbon nanotubes," *Chemistry Mater.*, vol. 16, no. 18, pp. 3414–3416, 2004.

[10] S. Li, Z. Yu, C. Rutherglen, and P. J. Burke, "Electrical properties of 0.4 cm long single walled carbon nanotubes," *Nano Lett.*, vol. 4, no. 10, pp. 2003–2007, 2004.
[11] S. Salahuddin, M. Lundstrom, and S. Datta, "Transport effects on signal propagation in quantum wires," *IEEE Trans. Electron Devices*, vol. 52, no. 8, pp. 1734–1742, Aug. 2005.
[12] Y. Wang, K. Kempa, B. Kimball, J. B. Carlson, G. Benham, W. Z. Li, T. Kempa, J. Rybczynski, A. Herczynski, and Z. F. Ren, "Receiving and transmitting light-like radio waves: Antenna effect in arrays of aligned carbon nanotubes," *Appl. Phys. Lett.*, vol. 85, no. 13, pp. 2607–2609, 2004.
[13] V. A. Podolskiy, A. K. Sarychev, and V. M. Shalaev, "Plasmon modes in metal nanowires and left-handed materials," *J. Nonlinear Opt. Phys. Mater.*, vol. 11, no. 1, pp. 65–74, 2002.
[14] ——, "Plasmon modes in metal nanowires and left-handed materials," *J. Nonlinear Opt. Phys. Mater.*, vol. 11, no. 3, pp. 339–339, 2002.
[15] ——, "Plasmon modes and negative refraction in metal nanowire composites," *Opt. Expr.*, vol. 11, no. 7, pp. 735–745, 2003.
[16] S. M. Huang, X. Y. Cai, C. S. Du, and J. Liu, "Oriented long single walled carbon nanotubes on substrates from floating catalysts," *J. Phys. Chemistry B*, vol. 107, no. 48, pp. 13 251–13 254, 2003.
[17] S. M. Huang, X. Y. Cai, and J. Liu, "Growth of millimeter-long and horizontally aligned single-walled carbon nanotubes on flat substrates," *J. Amer. Chemical Soc.*, vol. 125, no. 19, pp. 5636–5637, 2003.
[18] S. M. Huang, B. Maynor, X. Y. Cai, and J. Liu, "Ultralong, well-aligned single-walled carbon nanotube architectures on surfaces," *Advanced Mater.*, vol. 15, no. 19, pp. 1651–1655, 2003.
[19] S. M. Huang, M. Woodson, R. Smalley, and J. Liu, "Growth mechanism of oriented long single walled carbon nanotubes using "fast-heating" chemical vapor deposition process," *Nano Lett.*, vol. 4, no. 6, pp. 1025–1028, 2004.
[20] S. M. Huang, Q. Fu, L. An, and J. Liu, "Growth of aligned swnt arrays from water-soluble molecular clusters for nanotube device fabrication," *Phys. Chemistry Chem. Phys.*, vol. 6, no. 6, pp. 1077–1079, 2004.
[21] L. X. Zheng, M. J. O'Connell, S. K. Doorn, X. Z. Liao, Y. H. Zhao, E. A. Akhadov, M. A. Hoffbauer, B. J. Roop, Q. X. Jia, R. C. Dye, D. E. Peterson, S. M. Huang, J. Liu, and Y. T. Zhu, "Ultralong single-wall carbon nanotubes," *Nature Mater.*, vol. 3, no. 10, pp. 673–676, 2004.
[22] S. K. Doorn, L. X. Zheng, M. J. O'Connell, Y. T. Zhu, S. M. Huang, and J. Liu, "Raman spectroscopy and imaging of ultralong carbon nanotubes," *J. Phys. Chemistry B*, vol. 109, no. 9, pp. 3751–3758, 2005.
[23] B. H. Hong, J. Y. Lee, T. Beetz, Y. M. Zhu, P. Kim, and K. S. Kim, "Quasi-continuous growth of ultralong carbon nanotube arrays," *J. Amer. Chem. Soc.*, vol. 127, no. 44, pp. 15 336–15 337, 2005.
[24] T. Durkop, S. A. Getty, E. Cobas, and M. S. Fuhrer, "Extraordinary mobility in semiconducting carbon nanotubes," *Nano Lett.*, vol. 4, no. 1, pp. 35–39, 2004.
[25] W. Kim, H. C. Choi, M. Shim, Y. M. Li, D. W. Wang, and H. J. Dai, "Synthesis of ultralong and high percentage of semiconducting single-walled carbon nanotubes," *Nano Lett.*, vol. 2, no. 7, pp. 703–708, 2002.
[26] A. Bachtold, P. Hadley, T. Nakanishi, and C. Dekker, "Logic circuits with carbon nanotube transistors," *Science*, vol. 294, no. 5545, pp. 1317–1320, 2001.
[27] V. Derycke, R. Martel, J. Appenzeller, and P. Avouris, "Carbon nanotube inter- and intramolecular logic gates," *Nano Lett.*, vol. 1, no. 9, pp. 453–456, 2001.
[28] A. Javey, Q. Wang, A. Ural, Y. M. Li, and H. J. Dai, "Carbon nanotube transistor arrays for multistage complementary logic and ring oscillators," *Nano Lett.*, vol. 2, no. 9, pp. 929–932, 2002.
[29] Y. Huang, X. F. Duan, Y. Cui, L. J. Lauhon, K. H. Kim, and C. M. Lieber, "Logic gates and computation from assembled nanowire building blocks," *Science*, vol. 294, no. 5545, pp. 1313–1317, 2001.
[30] K. V. Pham, "Interface resistances and AC transport in a Luttinger liquid," *Eur. Phys. J. B*, vol. 36, no. 4, pp. 607–618, 2003.
[31] I. Safi and H. J. Schulz, "Transport in an inhomogeneous interacting one-dimensional system," *Phys. Rev. B*, vol. 52, no. 24, pp. 17 040–17 043, 1995.
[32] V. V. Ponomarenko, "Frequency dependences in transport through a Tomonaga-Luttinger liquid wire," *Phys. Rev. B*, vol. 54, no. 15, pp. 10 328–10 331, 1996.
[33] V. A. Sablikov and B. S. Shchamkhalova, "Dynamic conductivity of interacting electrons in open mesoscopic structures," *Jetp Lett.*, vol. 66, no. 1, pp. 41–46, 1997.
[34] Y. M. Blanter, F. W. J. Hekking, and M. Buttiker, "Interaction constants and dynamic conductance of a gated wire," *Phys. Rev. Lett.*, vol. 81, no. 9, pp. 1925–1928, 1998.
[35] G. Cuniberti, M. Sassetti, and B. Kramer, "AC-conductance of one-dimensional, long-range correlated electrons," *Phys. B*, vol. 227, no. 1–4, pp. 256–258, 1996.
[36] ——, "Transport and elementary excitations of a luttinger liquid," *J. Physics-Condensed Matter*, vol. 8, no. 2, pp. L21–L26, 1996.
[37] M. Sassetti and B. Kramer, "Spatial properties of nonlinear AC transport in a Luttinger liquid with an impurity," *Phys. Rev. B*, vol. 54, no. 8, pp. R5203–R5206, 1996.
[38] G. Cuniberti, M. Sassetti, and B. Kramer, "AC conductance of a quantum wire with electron-electron interactions," *Phys. Rev. B*, vol. 57, no. 3, pp. 1515–1526, 1998.
[39] V. A. Sablikov and B. S. Shchamkhalova, "Dynamic transport of interacting electrons in a mesoscopic quantum wire," *J. Low Temperature Phys.*, vol. 118, no. 5–6, pp. 485–494, 2000.
[40] P. J. Burke, I. B. Spielman, J. P. Eisenstein, L. N. Pfeiffer, and K. W. West, "High frequency conductivity of the high-mobility two-dimensional electron gas," *Appl. Phys. Lett.*, vol. 76, no. 6, pp. 745–747, 2000.
[41] S. Kang, P. J. Burke, L. Pfeiffer, and K. W. West, "Ballistic transport at GHz frequencies in ungated hemt structures," *Solid State Electron.*, vol. 48, no. 10, pp. 2013–2017, 2004.
[42] S. M. Kang, P. J. Burke, L. N. Pfeiffer, and K. W. West, "AC ballistic transport in a two-dimensional electron gas measured in gaas/algaas heterostructures," *Phys. Rev. B*, vol. 72, no. 16, p. 165312, 2005.
[43] S. Dassarma and A. Madhukar, "Collective modes of spatially separated, 2-component, two-dimensional plasma in solids," *Phys. Rev. B*, vol. 23, no. 2, pp. 805–815, 1981.
[44] C. A. Balanis, *Antenna Theory: Analysis and Design*, 2nd ed. New York: Wiley, 1997.
[45] S. Silver, *Microwave Antenna, Theory and Design*, 1st ed. New York: McGraw-Hill, 1949, 24 cm.
[46] S. DasSarma and E. H. Hwang, "Dynamical response of a one-dimensional quantum-wire electron system," *Phys. Rev. B*, vol. 54, no. 3, pp. 1936–1946, 1996.
[47] O. M. Yevtushenko, G. Y. Slepyan, S. A. Maksimenko, A. Lakhtakia, and D. A. Romanov, "Nonlinear electron transport effects in a chiral carbon nanotube," *Phys. Rev. Lett.*, vol. 79, no. 6, pp. 1102–1105, 1997.
[48] G. Y. Slepyan, S. A. Maksimenko, A. Lakhtakia, O. M. Yevtushenko, and A. V. Gusakov, "Electronic and electromagnetic properties of nanotubes," *Phys. Rev. B*, vol. 57, no. 16, pp. 9485–9497, 1998.
[49] A. Lakhtakia, G. Y. Slepyan, S. A. Maksimenko, A. V. Gusakov, and O. M. Yevtushenko, "Effective medium theory of the microwave and the infrared properties of composites with carbon nanotube inclusions," *Carbon*, vol. 36, no. 12, pp. 1833–1839, 1998.
[50] G. Y. Slepyan, S. A. Maksimenko, A. Lakhtakia, O. Yevtushenko, and A. V. Gusakov, "Electrodynamics of carbon nanotubes: Dynamic conductivity, impedance boundary conditions, and surface wave propagation," *Phys. Rev. B*, vol. 60, no. 24, pp. 17 136–17 149, 1999.
[51] G. Y. Slepyan, N. A. Krapivin, S. A. Maksimenko, A. Lakhtakia, and O. M. Yevtushenko, "Scattering of electromagnetic waves by a semi-infinite carbon nanotube," *Aeu-Int. J. Electronics Commun.*, vol. 55, no. 4, pp. 273–280, 2001.
[52] G. Y. Slepyan, S. A. Maksimenko, A. Lakhtakia, and O. M. Yevtushenko, "Electromagnetic response of carbon nanotubes and nanotube ropes," *Synthetic Metals*, vol. 124, no. 1, pp. 121–123, 2001.
[53] J. Appenzeller, R. Martel, P. Solomon, K. Chan, P. Avouris, J. Knoch, J. Benedict, M. Tanner, S. Thomas, K. L. Wang, and J. A. del Alamo, "A 10 nm mosfet concept," *Microelectronic Eng.*, vol. 56, no. 1–2, pp. 213–219, 2001.
[54] J. D. Kraus, *Antennas*, ser. McGraw-Hill series in electrical engineering, radar and antennas, 2nd ed. New York: McGraw-Hill, 1988.
[55] G. W. Hanson, "Fundamental transmitting properties of carbon nanotube antennas," *IEEE Trans. Antennas Propagat.*, vol. 53, no. 11, pp. 3426–3435, Nov. 2005.

Peter J. Burke (M'02) received the Ph.D. degree in physics from Yale University, New Haven, CT, in 1998.

From 1998 to 2001, he was a Sherman Fairchild Postdoctoral Scholar in physics at the California Institute of Technology. Since 2001, he has been a faculty member in the Department of Electrical Engineering and Computer Science, University of California, Irvine.

Shengdong Li (M'04) received the M.S. degree in electrical engineering from the University of California, Irvine (UCI), in 2004. He is currently working toward the Ph.D. degree in electrical engineering at UCI.

Zhen Yu (M'05) is working toward the Ph.D. degree in the Electrical Engieering and Computer Science Department, University of California, Irvine.